Front. Energy 2019, 13(4): 770–797
https://doi.org/10.1007/s11708-019-0651-x

REVIEW ARTICLE

Shammya AFROZE, AfizulHakem KARIM, Quentin CHEOK, Sten ERIKSSON, Abul K. AZAD

Latest development of double perovskite electrode materials for solid oxide fuel cells: a review

Abstract Recently, the development and fabrication of electrode component of the solid oxide fuel cell (SOFC) have gained a significant importance, especially after the advent of electrode supported SOFCs. The function of the electrode involves the facilitation of fuel gas diffusion, oxidation of the fuel, transport of electrons, and transport of the byproduct of the electrochemical reaction. Impressive progress has been made in the development of alternative electrode materials with mixed conducting properties and a few of the other composite cermets. During the operation of a SOFC, it is necessary to avoid carburization and sulfidation problems. The present review focuses on the various aspects pertaining to a potential electrode material, the double perovskite, as an anode and cathode in the SOFC. More than 150 SOFCs electrode compositions which had been investigated in the literature have been analyzed. An evaluation has been performed in terms of phase, structure, diffraction pattern, electrical conductivity, and power density. Various methods adopted to determine the quality of electrode component have been provided in detail. This review comprises the literature values to suggest possible direction for future research.

Keywords double perovskites, electrode materials, hydrocarbon fuel, solid oxide fuel cells

Received May 29, 2019; accepted Aug. 26, 2019; online Nov. 30, 2019

Shammya AFROZE, AfizulHakem KARIM, Quentin CHEOK, Abul K. AZAD (✉)
Faculty of Integrated Technologies, Universiti Brunei Darussalam, Jalan Tunku Link, Gadong BE 1410, Brunei Darussalam
E-mail: abul.azad@ubd.edu.bn

Sten ERIKSSON
Department of Chemistry and Chemical Engineering, Energy and Materials, Environmental Inorganic Chemistry, Chalmers University of Technology, Goteborg SE 41296, Sweden

1 Introduction

Fuel cells are one of the indispensable empowered technologies for next generation hydrogen energy production [1–3]. These cells are very efficient providers of electric power, generating electrical energy from chemical energy with no combustion [4,5]. The annals of the fuel cell have covered almost two centuries [2]. Nowadays the application of the fuel cell technology is the most important for its successful installation, mainly because of its working temperature (T), efficiency (η), start-up time and dynamic behavior [6], and the availability of fuel. Fuel cells applications are replacing internal combustions engines, providing both stationary power and portable power due to its very low or zero emissions [7]. For combustion-based technologies, these cells are used to generate the electrical power for all sorts of gadgets that are used every day [8].

As an illustration, the European Union wants to transfer all its energy system, including transport, into low-carbon systems by 2050 to reduce greenhouse gas emissions. Even Japan wants the 2020 Summer Olympics to be held in Tokyo to run on the renewable energy mainly produced from hydrogen fuel cells. Both Toyota and Honda are making fuel cell cars, because the preferable energy density of the fuel cell cars, in comparison with batteries, will have a great benefit in the long run [9]. Nissan also has its SOFC car which run on bioethanol [10]. Figure 1 shows the annual transport cells in different regions of the whole world [11].

The proton exchange membrane fuel cell (PEMFC), direct methanol fuel cell (DMFC), alkaline fuel cell (AFC), phosphoric acid fuel cell (PAFC), molten carbonate fuel cell (MCFC), microbial fuel cell, and solid oxide fuel cell (SOFC) have been used as different types of fuel cells [12], of which, the SOFC has gained more attention in the world market due to its high efficiency and longer lifetime [13]. The higher operating temperature of the SOFC sometimes acts as an obstacle in its applications, but this high temperature SOFC can reform the fuel internally [14]. In

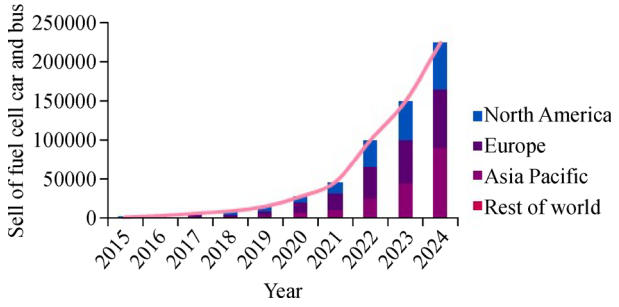

Fig. 1 Annual fuel cell cars and buses that had been (and will be) sold from 2015 to 2024 in world market in these regions.

fact, not only hydrogen but also a wide variety of fuel sources such as natural gas, biogas or other renewable fuels can be used as the fuel in the SOFC [15]. This cell can produce electricity using existing gas transmission infrastructure, making it ideal for electricity generation [16].

Why is SOFC? To mitigate environmental degradation, the world is searching for new fuel sources which will not emit any toxins like CO_2, SO_2 or NO_x, in the atmosphere [17]. People are being attracted to SOFC by its potential benefits. China has already taken one step ahead to overcome this polluted environment. In the USA, several SOFC companies have been established in recent years. Bloom Energy, Precision, Combustion, MO-SCI Corp., PolarOnyx, Inc., Lynntech, Inc., UES, Inc., Lupine Labs (fka FAST Ceramics), NexTech Materials, Sonata LLC, Protonex, Acumentrics, MEL Chemicals, FuelCell Energy, Yanhai Power LLC, ATREX ENERGY, INC., Si Energy Systems, Catacel, and Ztek are known by their names [18], whose main target is to move people away from dependence on polluting fuels and to provide clean, quiet, and efficient energy, as well as to lower manufacturing cost. The global SOFC market is estimated to be USD 403.4 million in 2017 and is projected to grow at a CAGR of 13.88% from 2017 to 2025 to reach a market size of USD 1140.6 million by 2025. Figure 2 describes the raising global demand to use the SOFC in the world market [19–20].

SOFC attracts researchers by its promising capabilities. Many scientists are now working on the evolution of new materials that can accomplish stability under operating conditions as well as catalytically active. They want to use that stable material at a reduced temperature while still enacting the desired stability, durability, and high performance of the SOFC. They also want to make the key components of the SOFC that are much cheaper to sharply curtail its overall cost. To gain a high electrocatalytic activity, the SOFC needs novel electrode materials that exhibit high performances [21]. Many materials have already been used to make conventional SOFCs, such as perovskite-type oxides, fluorites, etc. [22]. Recently research hubs show their keen interest in double perovskite electrode materials for their promising characteristics, for instance, high performance and stability with various fuels [23–25].

This review mainly focuses on electrodes in the SOFC with different double perovskite materials which have been used before, as well as their structures and performances. Besides, it discusses the challenges in using these perovskite materials and the new combination of novel materials in the SOFC.

2 Overview of SOFC

SOFC has become an expedient technology for electrical power generation due to its high-energy conversion efficiency, wide application range, fuel flexibility, and scant pollution [26–28]. Fuels, for instance, hydrogen and hydrocarbons can be used to spawn electricity in the SOFC as this cell is operated at high temperatures of 500°C–1000°C. Especially, when using hydrocarbon fuels such as natural gas to produce electricity, it has been recognized to be the most promising device with high energy conversion efficiencies [29,30]. It can generate more electricity than any other fuel cells of around 100 kW. Owing to high operating temperature, it has to face some hindrance like high costs, slow start-up time, high degradation rates, etc. The SOFC is especially well suited for power plants to provide a continuous stream of energy to industry as well as to a whole city [31].

The main advantage of the SOFC is the direct utilization of hydrocarbon fuels without any pretreatment [32–34]. More abundant hydrocarbon fuels such as natural gas have attracted researchers to do more work on the advancement of anode materials of SOFCs that operate directly on low cost. Solid ceramic electrolytes are used in the SOFC rather than a liquid one. The anode is fed with fuel where oxidation transpires and the reduction takes place in the cathode [28,35]. The new, eco-friendly demeanor deserves more attention and grandeur for the fuels as only hydrogen and oxygen are fed to the cell [36]. Hydrogen naturally exists in the atmosphere without releasing any toxins in the environment. It is found in the greatest quantities as water on earth. Pure hydrogen is used as fuel which is the most copious element on earth and can also be produced from biomass [37]. High reactivity with a suitable catalyst, high energy density, and the production of water only at the anode side make it capable of being used as fuel as the fuel is oxidized at the anode [38,39]. We can either split water or use hydrocarbon as a fuel. Direct use of hydrocarbons is very alluring and cost-effective [28]. Nowadays, CH_4 is also a popular fuel for SOFCs due to its availability. Generally, the oxidation reaction occurring within the SOFC at the anode can be written as

$$CH_4 + 4O^{2-} \rightleftarrows CO_2 + 2H_2O + 8e^- \quad (1)$$

In fact, the methane in this reaction breaks down and

forms CO_2. This oxidation reaction takes some steps to complete. For example,

$$CH_4 + 3O^{2-} \rightleftarrows CO + 2H_2O + 6e^- \quad (2)$$

The oxide-electrode surface is followed by reaction (3) and the competing reaction (4)

$$CO + O^{2-} \rightleftarrows CO_2 + 2e^- \quad (3)$$

$$2CO \rightleftarrows C + CO_2 \quad (4)$$

Reaction (4) results in the formation of carbon-carbon bond between two carbon atoms and is known as Boudouard reaction. Reaction (3) can be faster compared with reaction (4) on an oxide anode. The electrode surface may remain free from formation of coking. In reaction (4), disproportionation is clearly observed, which means no carbon deposition has occurred here. The steam of gas feeding through the anode usually removes CO from the surface. Reaction (5) can be expressed by reaction (6)

$$CO + H_2O \rightleftarrows CO_2 + H_2 \quad (5)$$

$$H_2 + O^{2-} \rightleftarrows H_2O + 2e^- \quad (6)$$

A typical SOFC is shown in Fig. 3 where it consists of two compartments of electrodes, namely the anode and cathode with an electrolyte embedded in between. An electrolyte for the SOFC requires a high ionic conductivity, a low electronic conductivity, a fully dense structure, a good mechanical strength, and a long duration stability [40]. The electrolytes of SOFCs can be either oxide ion conducting (Fig. 3(a)) or proton conducting (Fig. 3(b)) depending on their materials.

In the case of an oxygen-ion conductor, the movement of oxygen ion controls the current. However, the reaction products dilute the fuel. In proton conductor based SOFC, water will form on the cathode side, attenuating the air, not the fuel. Water is produced on the cathode side of the cell rather than the anode as shown in Fig. 3. First hand use of carbon-containing fuels is no longer possible with proton-conducting electrolytes because these materials show impermeability to gases [41–43].

The SOFC needs to lower its operating temperature for inexpensive materials used in the cell to make it more affordable because cheaper materials can be used at a low operating temperature for the components of the SOFC. These materials will also allow for a longer lifespan and less degradation. But with reducing temperatures, its performance decreases [44]. Generally, a SOFC is made up of four layers, of which three are composed of ceramic materials such as, anodes, cathodes, and electrolytes and the interconnect, as the fourth part, is usually incorporated with metal or ceramic layer which is placed between each cell in the SOFC stack. Figure 4 is a schematic diagram of a SOFC stack [48].

Anode: The main responsibilities of the anode materials in SOFCs are to facilitate the oxidation of the fuel and the transport of electrons from the electrolyte to the fuel/electrode interface.

Electrolyte: Electrolyte in the SOFC needs a very fast ionic transport, a very low electronic conductivity, thermodynamic stability and stability under oxidizing and reduction atmospheres. These materials must possess the thermal expansion compatible with that of the electrodes and other construction materials, high density, negligible volatilization of components, suitable mechanical properties and negligible interaction with electrode materials under operation conditions [45]. The conductivity of the electrolyte determines the operating temperature of SOFCs.

Cathode: Pure oxygen or oxygen from the air is reduced to oxygen ions (O^{2-}) in the cathode. Electronic conducting oxide materials are used as cathode due to the high operating temperature [46].

Interconnect: The interconnect must be both chemically

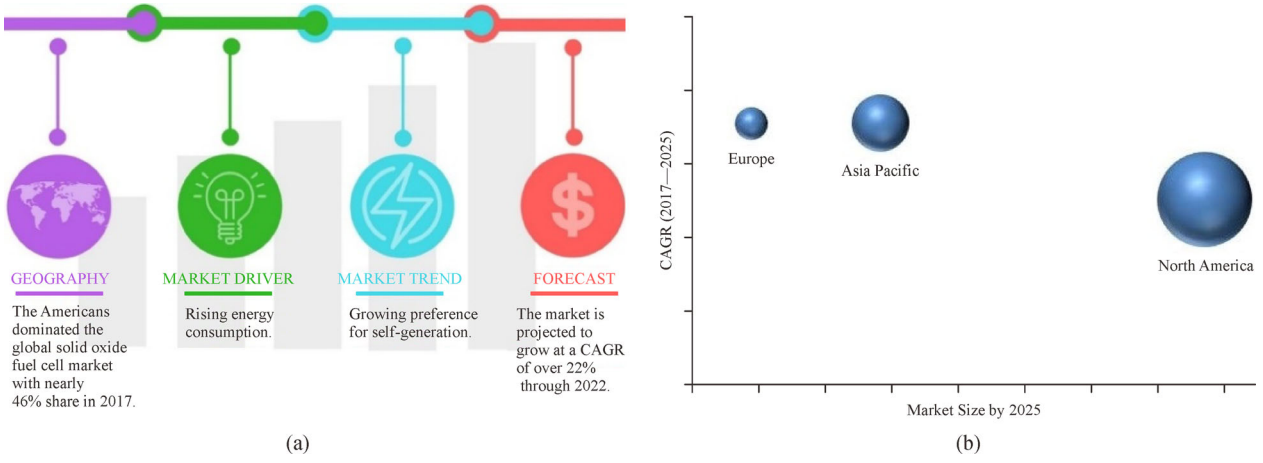

Fig. 2 Raising global demand to use SOFC in the world market.
(a) Top emerging trends in global SOFC market; (b) SOFC market progress in the world by 2025.

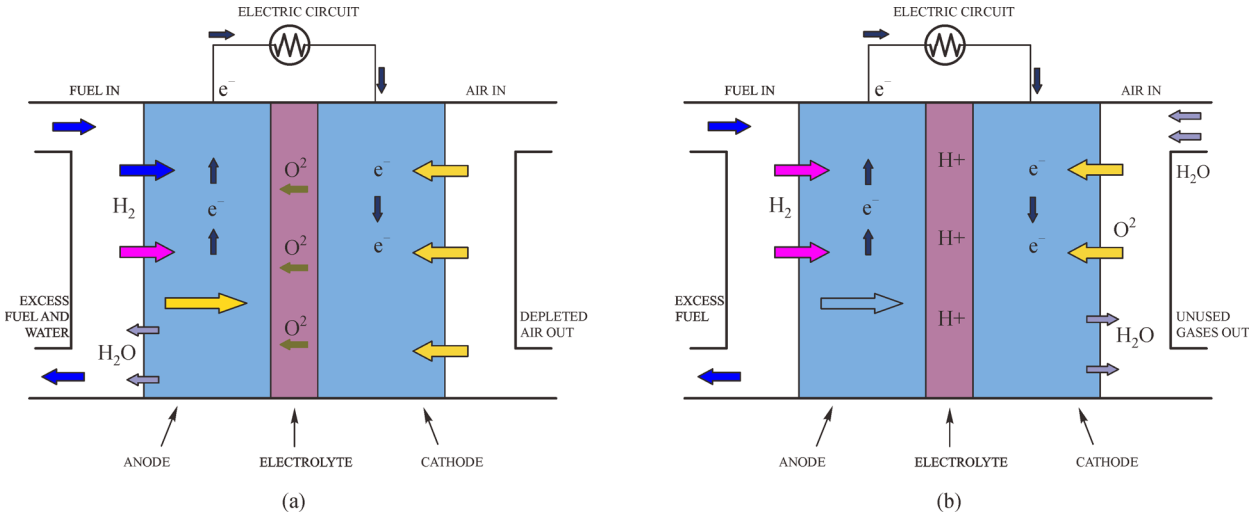

Fig. 3 Schematic diagram of SOFC.
(a) Oxide-ion conducting electrolyte; (b) proton conducting electrolyte (adapted with permission from Ref. [41]).

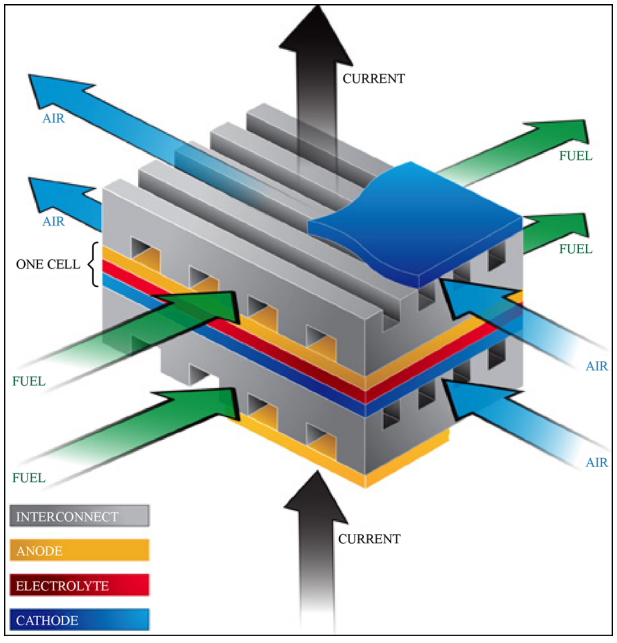

Fig. 4 Schematic diagram of SOFC stack.

and physically stable in reducing and oxidizing environments, have good electronic conductivity, have sufficient strength to support other cells, and be easily fabricated into the required configuration [47].

Since the SOFC works at very high temperatures, probably the highest temperature of all types of the fuel cell, at around 800°C to 1000°C, it can have the competence of over 60% when converting fuel to electricity. If the heat produced by the SOFC can be used, the overall efficiency can inflate up to more than 80%. Recently the SOFC is being tested to be used in individual homes or buildings with a micro-CHP system [49,50] which can help to alleviate some of the strain placed upon the grid by the expansion of electrification in other areas. The use of the SOFC micro-CHP system in Germany, Italy, the UK and Poland are escalated. The company named Solid Power with BlueGen unit is producing home-scale micro-CHP systems [51]. Figure 5 illustrates the advantages and disadvantages of the SOFC.

3 Perovskite and double perovskite

Nowadays perovskite-type materials are most promising anode material used in the SOFC for their attractive ionic and catalytic property [52], superconductivity [53], magneto resistance [54], ferroelectric, piezoelectric [55] and pyroelectrical properties. The leading research hub is focusing on perovskite because almost all the metals in the periodic table can integrate on the *A*-site or *B*-site element. The elements that can occupy in *A*-, *B*-, *X*-sites are as follows [56].

A: Sr, Ba, Na, K, Rb, Cs, Y, Ag, Pb, Bi and some rear earth materials like Nd, La, Sm, Gd, Pr, Yb, and Ce;

B: Mg, Cu, Ni, Fe, Co, Cr, V, W, Zn, Ga, Rh, Al, Si, Sc, Ti, Cr, Mn, Mo, Zr, Fe, Zr, Nb, Yb, Sn, Hf, Ta, and U;

X: O, H, F, S, Cl, Se, and Br.

The general formula for an optimal perovskite can be written as ABX_3, where the *A*-site cations are typically larger than the *B*-site cations and similar in size to the *X*-site anions as depicted by $A^{2+}B^{4+}O_3$ or $A^{1+}B^{5+}O_3$, or $A^{3+}B^{3+}O_3$ [57].

The structural configuration of this perovskite can be considered as a face-centered cubic lattice (FCC), where the *A* atom is situated at the corner with 12 coordination numbers, the *B* atom located at the lattice center with 6 coordination numbers, the *X* atom pinpointed on the faces

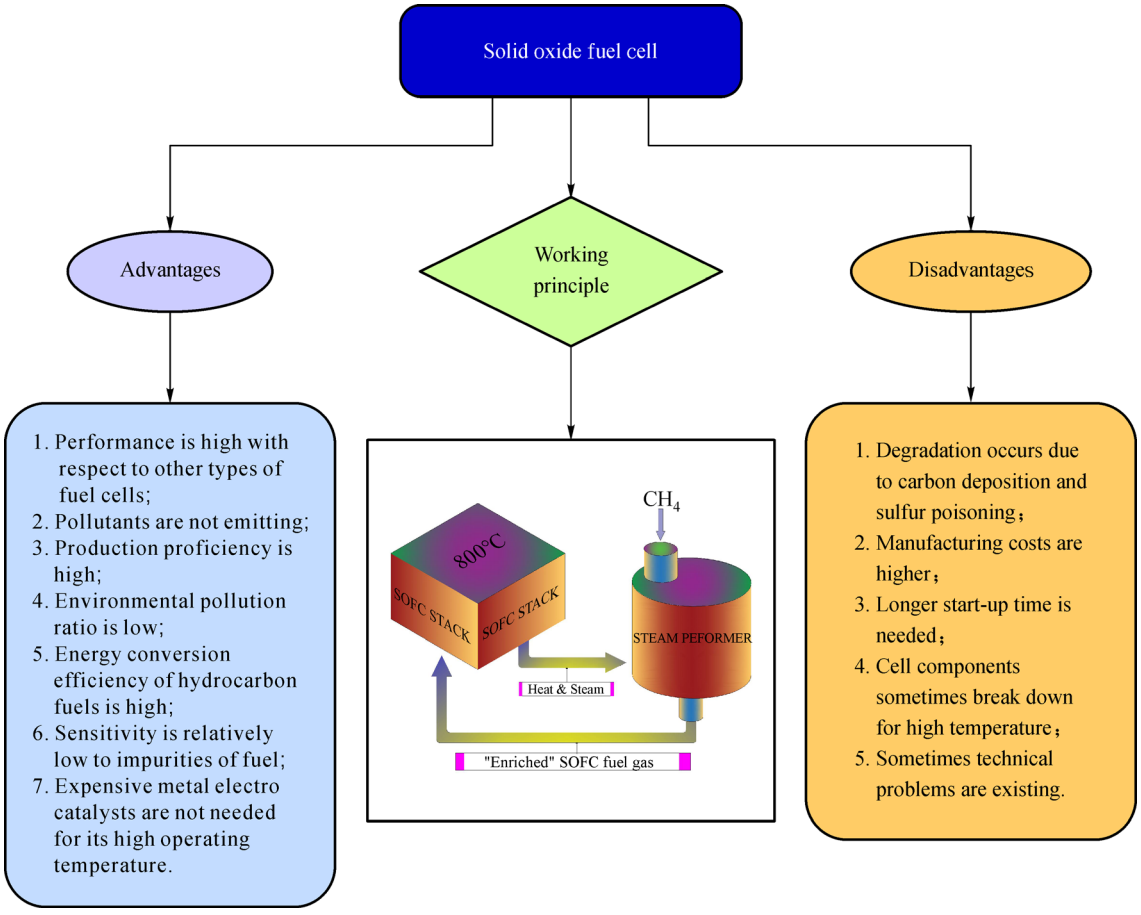

Fig. 5 Advantages and disadvantages of SOFC with its working principle.

of the lattice mentioned above. The perovskite structure is completed by the *B* atom which stays in the form of BO_6 octahedron. The largest atom is the *A*-site one which is responsible for the increase of the volume of the whole unit cell. The ideal perovskite structure is a three-dimensional system of connections of octahedron named BO_6, with the more ample size of *A*-cations occupying 12 coordinated voids to fill the space between the octahedron. The perovskite structure can accommodate a large number of anion vacancies which facilitate the electronic/ionic conduction. This structure can also have a large amount of tilting/distortion and can be found in seven types of Bravais lattices (cubic or triclinic). The physical properties depend not only on the constituting elements but also their arrangement in the structure. In many cases, the thermal resistance depends on the *A*-site cation while the catalytic activity depends on the *B*-site [58,59]. Figure 6(a) shows the *B*-site cation with 6 coordination numbers and the *A*-site cation with 12 coordination numbers, while Fig. 6(b) demonstrates its ordered double perovskite arrangement [60]. The three structural degrees of freedom of perovskites are as follows:

(a) *A* and *B* cation displacement from the centers;

(b) The polyhedral distortion of the coordination around *A* and *B* ions;

(c) The BX_6 octahedra tilting with respect to one, two, or three axes.

An ordered rock-salt-like arrangement of corner-sharing BO_6 and $B'O_6$ units in the crystal structure, e.g., $A_2BB'O_6$ or $AA'BB'O_6$, where *A*, *A*′, *B* and *B*′ are different elements, are termed as double perovskites [60]. This is formed when the alkali, alkaline earth, or rare earth ions are chosen for the *A*-site and the metal ions are chosen for the *B*- and *B*′-sites. Double perovskites can accommodate large amounts of oxygen non-stoichiometry and have been studied extensively for their magnetic properties [61–66]. The divalent *A*-cation permits a big range of oxidation state for the *B* and *B*′ cations. These two *B* cations need a convenient oxidation state to form the perovskite phase. In the case of A^{2+}cation, the total oxidation state of the *B* site will be four, which can also be adapted for B^{4+}/B^{4+}, B^{3+}/B^{5+}, B^{2+}/B^{6+}, and B^{+}/B^{7+}. For $A_2{}^{2+}BB'O_6$, the oxidation states in the *B* site range from 1 to 7. Thus in the case of A^{3+}cation, the *B* site combination will be B^{3+}/B^{3+}, B^{2+}/B^{4+}, and B^{+}/B^{5+}. For the A^{3+} cation, the average oxidation state of the *B* site is three. But for the A^{+} cation, the ionic radii are large. Therefore, the *B* site oxidation state will be B^{5+}/B^{5+}, B^{4+}/B^{6+}, and B^{3+}/B^{7+}.

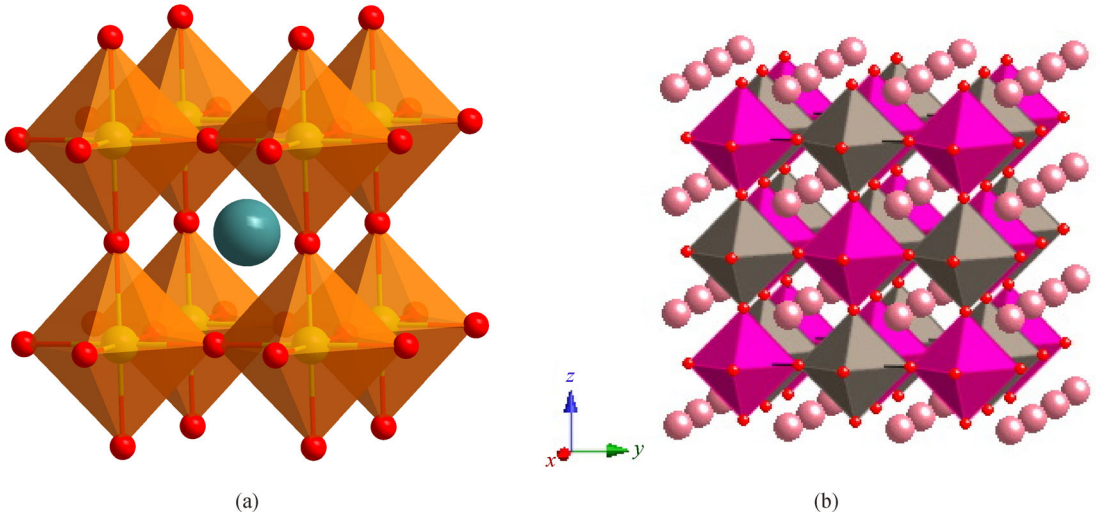

Fig. 6 Schematic 3D representation of perovskite structure.
(a) A general basic perovskite structure (space group: *Pm*-3*m*) showing the octahedral (6-coordinated) and cubo-octahedral (12-coordinated) of the *B*- and *A*-site cations, respectively; (b) ideal 1:1 double perovskite in cubic symmetry (space group *Fm*-3*m*, $a = 2a_p$).

According to Huang et al., $Sr_2MgMoO_{6-\delta}$(SMMO) is highly attractive because of its redox stability, proper thermal expansion coefficient compared to the standard solid electrolytes, and excellent electrocatalytic activity toward natural gas used directly as fuel [67–69]. At the same time, Marrero-López et al. [70] and Bernuy-Lopez et al. [71] have found that SMMO under 5% hydrogen reducing atmospheres has a high redox stability of up to 900°C. Meanwhile, Sr_2MMoO_6 (M = Co,Ni) series, as anode materials, have been reported [72], which exhibit a high cell power density in the hydrogen and methane atmosphere. Unfortunately, SMMO based double perovskite showed a lower electrical conduction and hence giving a higher unfavorable anode polarization. Nonetheless, doping with donor or acceptor on *A* or *B* sites does help in the electronic or ionic conductivity of Sr_2MgMoO_6 via the introduction of various ionic and electronic defects. The electrocatalytic properties for fuel oxidation could also be improved by modifying SMMO by substituting the Sr with La^{3+} ions but the structural ability deteriorates at high oxygen partial pressure [73]. Meanwhile, the Mg-site can be doped with Mn, thus increasing the electrical conductivity. However, Mn-doped is much sensitive to pO_2 and the electrical conductivity decreases as the partial pressure of oxygen increases [74]. Fe, Al, and Co-substituted SMMO have also been investigated to find the suitability of the material under redox conditions [75–77].

For pure perovskite structures, the relative size of the *A* and *B* site cations determines the stability of the perovskite slab. The *A*-O bond length is equal to $\sqrt{2}$ and *B*-O is normally 40% smaller than *A*-O bond length. In the case of perovskite, the Goldschmidt tolerance factor (t) which is the mismatch of the size of *A*- and *B*-cations can be described as

$$t = \frac{r_A + r_O}{\sqrt{2}(r_B + r_O)},$$

where r_A, r_B, and r_O are the ionic radii of *A*, *B*, and *O* respectively.

For double perovskites, the Goldschmidt tolerance factor t [78] can be written as

$$t = \frac{(r_{a'} + r_{a''})/2 + r_O}{\sqrt{2}x[(r_{b'} + r_{b''})/2 + r_O]},$$

where $r_{a'}$, $r_{a''}$, r_O, $r_{b'}$, and $r_{b''}$ are the Shannon ionic radii [79] of the constituent ions. The *A*-site cation radius is for the twelve-fold oxygen coordination, whereas the *B*-site radius is for the six-fold oxygen coordination. In fact, the perovskite structure may form in oxides for which $0.89 < t < 1.06$.

(1) When $t < 1$, the radius of the *A*-site cation is smaller than standard and the perovskite structure can atone for the size of the cation by tilting BO_6 octahedra;

(2) When $t > 1$, the radius of the *A*-site cation is immensely large. Therefore, the perovskite structure cannot be formed by tilting octahedral [80,81]. Even in this case, the structure can also be formed instead of tilting only to change the bond lengths (the *A*–O bond or the –O bond).

But sometimes the cation radii are not perceived. Therefore, the tolerance factor t cannot be calculated. In $A_2^{2+}BB'O_6$, the *A*-site cation can affect only the volume of the unit cell but the *B*-site cation involves the perovskite structure and space group found in the literature. Besides, for a single perovskite, only the *A*-*B* cation radii difference is important, but for the double perovskite structure, the *B*-

B' cation radii mismatch is very substantial. Table 1 lists the calculated tolerance factors of some double perovskite electrodes reported in literature and Fig. 7 plots the tolerance factor t versus the composition to find the trend. The reported electrodes have t values in the range of 0.88 to 1.08 [64,72,81–100]. A maximum in a number of electrodes is found around $t = 0.9$ to 1.01, where the ionic radii match is quite close to the ideal.

3.1 *A*-site doping

Various types of cations can be used to make different compositions to substitute *A*- or *B*-site or both sites. Perovskite-type oxides can be partial or totally reduced in the reductive atmosphere, depending on the *A*- and B-positions [101]. Thus, double perovskite materials can be made by substituting the *A*-site cation like $A_{1-x}A_xBB'O_6$ or by substituting the *B*-site cation, for instance, $A_2B_{1-x}B_x'O_6$, or by substituting both, such as $A_{1-x}A_xB_{1-x}B_x'O_6$.

Many studies have been conducted on *A*-site ordered double perovskites. Cation ordering on *A*-site actually affects the physical properties of double perovskites. For instance, Parfitt et al. have reported that oxygen self-diffusion in the double perovskite $GdBaCo_2O_{5+\delta}$ (GBCO), in which Gd or Ba cations align in alternating (001) layers, is strongly dependent upon the *A*-site cation order [102].

Table 1 Calculated tolerance factors of some double perovskite electrode materials

Electrodes	t	Electrodes	t	Electrodes	t
$Ba_{0.1}Sr_{1.9}NiWO_6$	0.985	Ca_2CrWO_6	0.945	$Sr_2MgMoO_{6-\delta}$	0.977
$Ba_{0.2}Sr_{1.8}NiWO_6$	0.988	Ca_2FeReO_6	0.970	$Sr_2MnMoO_{6-\delta}$	0.952
$Ba_{0.25}Sr_{1.75}NiWO_6$	0.989	$Ca_2FeMoO_{6-\delta}$	0.860	$Sr_2FeMoO_{6-\delta}$	0.963
$Ba_{0.3}Sr_{1.7}NiWO_6$	0.991	Ca_2CrSbO_6	0.880	$Sr_2CoMoO_{6-\delta}$	0.971
$Ba_{0.4}Sr_{1.6}NiWO_6$	0.994	Ca_2FeReO_6	0.963	$Sr_2NiMoO_{6-\delta}$	0.984
$Ba_{0.5}Sr_{1.5}NiWO_6$	0.997	Ca_2CoNbO_6	0.961	$Sr_2ZnMoO_{6-\delta}$	0.973
$Ba_{0.75}Sr_{1.25}NiWO_6$	1.004	Ca_2NiWO_6	0.947	Sr_2CrWO_6	0.999
$BaSrNiWO_6$	1.011	$Ca_{1.9}Sr_{0.1}NiWO_6$	0.949	Sr_2CeSbO_6	0.920
$Ba_{1.25}Sr_{0.75}NiWO_6$	1.019	$Ca_{1.8}Sr_{0.2}NiWO_6$	0.951	Sm_2LiOsO_6	0.900
$Ba_{1.5}Sr_{0.5}NiWO_6$	1.026	$Ca_{1.6}Sr_{0.4}NiWO_6$	0.954	Sr_2MnWO_6	0.949
Ba_2NiWO_6	1.041	$Ca_{1.5}Sr_{0.5}NiWO_6$	0.956	Sr_2NiWO_6	0.982
$BaY(Cu_{0.5}Fe_{0.5})_2O_5$	1.056	$Ca_{1.4}Sr_{0.6}NiWO_6$	0.958	A_2MnMoO_6 (A = Ba,Sr)	1.050
$BaRE_{1-x}La_xCo_{2-y}Fe_yO_{6-\delta}$	0.950–1.000	$Ca_{1.25}Sr_{0.75}NiWO_6$	0.960	La_2CuNiO_6	0.825
$Ba_{2-x}Sr_xMnReO_6$ (x = 0, 0.5, 1, 2)	1.000	$Ca_{1.2}Sr_{0.8}NiWO_6$	0.961	La_2NaIrO_6	0.890
$Ba_2FeMoO_{6-\delta}$	0.980	$CaSrNiWO_6$	0.965	Pr_2NaIrO_6	0.880
Ba_2CrWO_6	1.059	$Ca_{0.8}Sr_{1.2}NiWO_6$	0.968	Nd_2NaIrO_6	0.860
Ba_2LaSbO_6	0.960	$Ca_{0.6}Sr_{1.4}NiWO_6$	0.972	La_2LiOsO_6	0.930
Ba_2PrSbO_6	0.970	$Ca_{0.5}Sr_{1.5}NiWO_6$	0.973	Pr_2LiOsO_6	0.920
Ba_2NdSbO_6	0.971	$Ca_{0.4}Sr_{1.6}NiWO_6$	0.975	Nd_2LiOsO_6	0.910
Ba_2SmSbO_6	0.977	$Ca_{0.3}Sr_{1.7}NiWO_6$	0.977	Pb_2FeMoO_6	1.032
Ba_2FeReO_6	1.060	$Ca_{0.2}Sr_{1.8}NiWO_6$	0.979	La_2LiIrO_6	0.940
Ba_2CaWO_6	0.967			Pr_2LiIrO_6	0.930
Ba_2CaReO_6	0.979			Nd_2LiIrO_6	0.920
Ba_2CaOsO_6	0.980			Sm_2LiIrO_6	0.910
Ba_2CaUO_6	0.940			Eu_2LiIrO_6	0.900
Ba_2CaNpO_6	0.942				
Ba_2CaPuO_6	0.944				
Ba_2SrNpO_6	0.906				
Ba_2SrNpO_6	0.908				
Ba_2LaIrO_6	0.967				
Ba_2YIrO_6	0.997				

Even La or Ce-doped Sr_2NiMoO_6, reported by Sabrina Presto et al., has gained the high electrical conductivity which can be contemplated as one of the auspicious anode material for the SOFC running at operating temperature [103]. Doping in *A*-site gives good performance for SOFC electrode materials. As an illustration, $Pr_{1-x}Ca_xBaCo_2O_{5+\delta}$ (PCBCO) double perovskite exhibits very good electrochemical performance and chemical compatibility. The corresponding maximum power density values decreases from 646.5 mW/cm^2 at 800°C [104].

3.2 *B*-site doping

The materials need a high degree of cation ordering to accomplish the alluring properties of perovskites. Unfortunately, the assemblage of super lattices is a bit harder because of their slow growth, which hinders the industrial interest. For the *B*-site cation ordering in double perovskite, the similarity of the ionic formal valence and ionic radius are the major problems. Hence, to achieve a spontaneous *B*-site rock salt ordering in bulk, a distinct difference in FV and r_B is necessary [105]. B' and B'' cations are accountable for the ordering /disordering effect of perovskite. The charge difference of these cations is mainly encountered for this effect. The three *B*-site ordering sublattice in double perovskites are as follows (in Fig. 8).

These ordering phenomena always affect the physical properties of materials. The *B*-site cation ordering affects the half-metallic properties of $Sr_2(Fe_{1-x}Cr_x)ReO_6$ double perovskites [106]. For $PrBaCo_{2-x}Cu_xO_{5+\delta}$, Cu doping in the *B*-site aids the evolution of oxygen vacancies at a lower temperature [107]. Niu et al. [108] have measured the excellent performance at reduced atmosphere and found the coking resistant and sulfur tolerant anode material for the SOFC. The maximum power density is recorded for Ni-doped $NdBaCo_{2-x}Ni_xO_{5+\delta}$ at 700°C, 750°C, and 800°C and the electrical conductivity is around >300 S/cm up to 900°C [109]. Single crystals are most appropriate when examining the sublattice type and carrying out a structure analysis. Since it is often very difficult to obtain single crystals, powder diffraction data can be used (for most of the cases) to determine the types of sublattice. The determination of sublattice types is based on the size of the unit cell, systematic absences, crystal system, and other topological transformations. For some crystal structures, the arrangement cannot be made unambiguously, when powder diffraction data are used to determine the *B*-cation sublattice type. Neutron diffraction, electron diffraction microscopy or X-ray diffraction data from a synchrotron source can be used to ascertain the single crystal structure. The two main *B*-site cation sublattice types and common cell sizes, crystal systems, and space groups are shown in Table 2. Figure 9 shows a different kind of *B*-cation sublattices.

3.2.1 Random/partially ordered type

The difference between valance and ionic radius actually generates an order. Compounds having a random type sublattice generally form a cubic unit cell or an orthorhombic unit cell. The bond length is very important to form a random type sublattice to get either a cubic unit cell or an orthorhombic unit cell. Generally, the bond length *A*-O is less than $\sqrt{2}$ times the bond length *B*-O when the orthorhombic cell is formed. In Glazer's notation for $a^+b^-b^-$ or $a^+a^-a^-$, the rotation of BO_6 octahedron forms this cell [115]. Higher order reflections are absent for a cubic cell in random type sublattice. The reflections, *0hkl*: $k = 2n + 1$, are absent in orthorhombic cell. The most common space group observed for compounds that have random sublattice with orthorhombic symmetry is *Pbnm*.

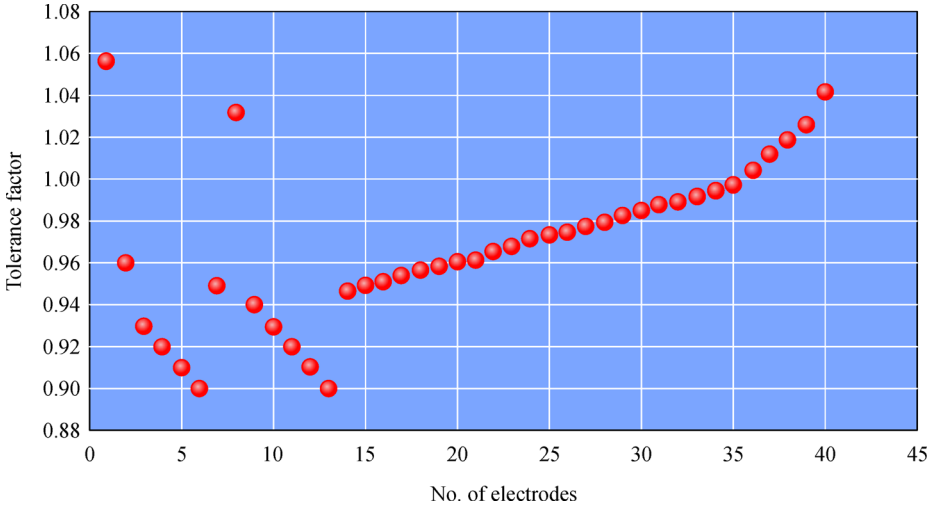

Fig. 7 Number of double perovskite electrodes reported with different values of tolerance factor *t*.

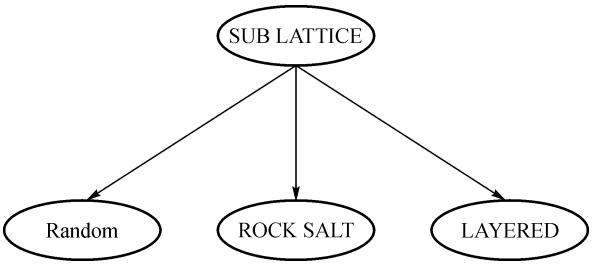

Fig. 8 *B*-cation sublattice types.

3.2.2 Rock salt type

The arrangement of the *B*-site cation is commensurate to the positions of anion and cation. The compounds having a rock salt type sublattice usually crystallize in a $2a_p$ cubic unit cell, for instance [112], Sr_2CuWO_6 [116] or a monoclinic $\sqrt{2}\,a_p\times\sqrt{2}\,a_p\times\sqrt{2}\,a_p$ unit cell, such as Ca_2MnWo_6 [65], Ca_2FeMoO_6 [117]. A monoclinic cell is found when the most common tilting found as $a^+b^-b^-$ in Glazer's notation or $a^+a^-a^-$. This cell stands with the minimum tolerance factor with a rotation of BO_6 octahedron where each octahedron is isolated from others. These types of compounds show the evidence of the *B*-site cation ordering. In a cubic cell, the cation ordering is different as the lattice parameter is doubled with respect to the cation for random distribution. Higher order reflection is observed in cubic cell. When the tolerance factor is quite large, the cubic diction takes place. To amend the *A*-site cation, bonding is the main purpose of octahedral tilting in rock salt type ordering.

3.2.3 Layered type

When the *B′* and *B″*cations can alternate in one direction, the layered type is formed. The monoclinic structure of a layered type double perovskite material, such as La_2CuSnO_6 [118], has $2a_p\times2a_p\times2a_p$unit cell. These three sublattice types are different from each other by the presence of the valance. For instance, the unit cell arrangement of layered type is $2a_p\times2a_p\times2a_p$, while the random arrangement is $a_p\times a_p\times a_p$. Even the rock salt type is quite different from the layered one as the BO_6 octahedron can rotate in two dimensions [105].

Layered type double perovskites with a large number of oxygen vacancies have been proved to be good electrode materials for the SOFC. Recent research focuses on lanthanide (Ln)-containing oxide materials doped with alkaline elements (Ba, Sr, Ca, etc.) and transition metals (Cr, Mn, Fe, etc.). Hence, their good mixed electronic and ionic conducting behavior are recognized as very promising (LT, IT, HT-SOFCs) for electrode materials. However, these materials still exhibit slow oxygen transportation kinetics, specifically at intermediate temperatures of

Table 2 Sublattice types, cell sizes, crystal system, and space groups of two main *B*-site cations

Sublattice type	Cell size	Cryatal system	Space group	Representative references
Random	$a_p\times a_p\times a_p$	Cubic	*Pm*-3*m*	[110]
	$2a_p\times\sqrt{2}a_p\times2a_p$	Orthorhombic	*Pbnm*	[111]
Ordered	$2a_p\times2a_p\times2a_p$	Cubic	*Fm*-3*m*[a]	[112]
	$\sqrt{2}a_p\times\sqrt{2}a_p\times2a_p$	Tetragonal	I4/m[a]	[62,113]
	$\sqrt{2}a_p\times\sqrt{2}a_p\times2a_p$	Monoclinic	$P2_1/n$[a]	[65]
	$2a_p\times2a_p\times2a_p$	Monoclinic	$P2_1/m$[b]	[114]

Notes: a—NaCl-type; b—layered type; a_p(~3.9Å) is the unit cell parameter of ideal cubic perovskite.

Fig. 9 **A** different kind of *B*-cation sublattices (adapted with permission from Ref. [105]).
(a) Random; (b) layered; (c) rock salt arrangement.

500°C–800°C. *A*-site layered perovskite $PrBaCoMn_2O_{5+\delta}$ [119] has been introduced with the structure-property relationship. Recently, a layered perovskite anode, $PrBaMn_2O_{5+\delta}$ has been demonstrated as a good redox stable with tolerance to coking and sulphurcontamination from hydrocarbon fuels $PrBaCo_2O_{5+\delta}$ is reported to have suitable electrical properties to use as a cathode in the SOFC [120]. In a recent study, the material of $NdBaMn_2O_{5+\delta}$ has been investigated with regard to its structure and electrical conductivity [21].

4 Exploring new electrodes for SOFC

Since the anode acts in reducing environment while the cathode is in oxidizing environment, the electrode material of a symmetrical SOFC has to take the challenge to demonstrate chemical and structural stability in both reducing and oxidizing environments and maintain the dual electrocatalytic performance for both oxygen reduction and fuel oxidation. Different types of oxides with perovskite, fluorite, and pyrochlore structures have already been investigated as potential redox stable electrode materials [121,122].

Anode is much more responsible for the performance and endurance of the SOFC. The anode requires reducing environment. The most commonly used anode material is the Ni-based composites which exhibit a good conductivity and a high performance for pure hydrogen oxidation [123]. However, Ni-based anode materials also demonstrate some detriments such as low tolerance to carbon unless a large amount of steam is added to reform the fuel, exposure to sulfur substantially existing in natural fuels [124], and nickel coarsening as well as poor volume stability upon redox cycling. To overcome these obstacles with maximizing the convenience of the intrinsic fuel flexibility of the SOFC, the development of anode materials should have to be concentrated on. Seungdoo Park et al. [125] have reported that Cu-CeO_2-YSZ composite anodes operated on a range of dry hydrocarbons can reduce carbon deposition and have a good sulfur tolerance. Cu particles are excellent electronic conductors but show a poor catalytic activity [126].

Anode materials should have the following basic requirements [127]:

(1) Porous anode (easy evacuation of hydrogen and formed water);

(2) The prerequisite of an anode in the SOFC is the excessive fuel flexibility that would receive feed sources such as natural gas, hydrogen, and other various light hydrocarbons;

(3) Relatively high electrical conductivity;

(4) High-temperature stability;

(5) Flexibility for electron and conduction;

(6) Fuel-flexible, ease of fabrication, and low cost;

(7) Thermal expansion coefficient (TEC) and chemical compatibility matched with the adjoining components;

(8) High wettability needed to compare with the electrolyte substrate;

(9) Excellent carburization and sulfidation resistance on using hydrocarbons as a fuel.

A lot of efforts have been made to synthesize and characterize these anode components to get ultimate cell performance.

In this section, a few structural and electrochemical parameters are focused on to compare the electrode (anode and cathode) materials investigated, such as diffraction pattern and space group with phase, electrical conductivity and power density. Table 3 tabulates the major characterization of some double perovskite anode materials used in the SOFC. The space group, phase, diffraction pattern, electrical conductivity (S/cm) and power density (mW/cm^2 –W/cm^2) acquired from literature are reported here.

For anode materials, the highest electrical conductivity is obtained for Ca_2FeMoO_6 with monoclinic (Table 3, Ref. [128]), while much lower conductivity value is reported in $Sr_{2-x}Ba_xMMoO_{6-\delta}$ (M = Co, Ni; x = 0, 0.5, 1.0, 1.5 and 2.0), $< 10^{-2}$ S/cm for Ni- containing materials at 800 C [129]. The highest power density value is obtained for 1066 mW/cm^2 at 800 C under humidified H_2 [130].

The thermal expansion coefficient plays a vital role in whole SOFC performance. The selection of cathode materials mainly depends on the electrolyte materials [161]. SOFC can be operated at a very low cell voltage to establish cathode durability. The partial pressure of O_2 at the cathode ternary phase boundary can be quite low for a redox stable cathode. Lanthanum strontium manganite, $(La,Sr)MnO_{3-\delta}$ (LSM), is a common cathode material for the SOFC. This material has a very high performance with its high electrochemical activity for the O_2 reduction reaction at high temperatures, a good thermal stability, chemical stability, and rapport with the electrolyte in the SOFC [162,163]. Though LSM has an excellent electrical conductivity, it has a low oxygen ionic conductivity [164]. For these reasons, the LSM component is not suitable for SOFC operation. For stability, significant efforts have been made to search for cathode materials with a high ionic conductivity operable at lower temperatures.

Kim et al. [165] have measured a very high electrical conductivity at a lower temperature and made the oxygen ion diffusion easily. Therefore it can be a good cathode for the SOFC. Some cathode materials execute chemical stability as well as high catalytic activity, and remain stable under CO_2 like $PrBa_{0.5}Sr_{0.5}Co_{1.5}Fe_{0.5}O_{5+\delta}$ (PBSCF) [166]. Table 4 shows the major characterizations of some double perovskite anode materials used in the SOFC.

The expected properties of a good cathode are as follows [167]:

(1) Higher electronic conductivity (ideally more than 100 S/cm under oxidizing ambience);

Table 3 Various types of methods, space group, phase, conductivity, and highest power density of double perovskite type anode materials fabricated for SOFC

Double perovskite anode materials	Space group	Phase	Diffraction pattern	Power density	Conductivity	Ref.
$Sr_2CoMoO_{6-\delta}$, $Sr_2NiMoO_{6-\delta}$, $Sr_2Fe_{1.5}Mo_{0.5}O_{6-\delta}$	*I*4/*m*	Tetragonal	XRD	–	–	[131]
$Sr_{2-x}Sm_xNiMoO_{6-\delta}$	*I*4/*m* $I4_1/a$ ($SrMoO_4$)	Tetragonal	XRD	–	–	[132]
$Sr_2FeNb_{0.2}Mo_{0.8}O_{6-\delta}$	*I*4/*mmm*	Tetragonal	XRD	–	19.5 S/cm in air and 5.3 S/cm in 5% H_2 at 800°C	[133]
Mo doped $Pr_{0.5}Ba_{0.5}MnO_{3-\delta}$(Mo-PBMO)		Cubic and hexagonal	XRD	700 mW/cm^2 at 850°C	101 S/cm in air at 800°C	[134]
A_2FeMoO_6 (AFMO, A = Ca, Sr, Ba)	$P2_1/n$ (CFMO), *P*4/*mmm*(SFMO) and *Fm*-3*m*(BFMO)	Monoclinic(CFMO), Tetragonal (SFMO) and cubic (BFMO)	XRD	0.20 mW/cm^2 (CFMO), 757 mW/cm^2(SFMO) and 605 mW/cm^2 (BFMO) at 850°C	306 S/cm for CFMO, 212 S/cm for SFMO and 191 S/cm for BFMO in 5% H_2 at 850°C	[128]
$PrBaMn_2O_{5+\delta}$	*P*4/*mmm*	Tetragonal	NDP	–	–	[135]
$SrLaFeO_4$ ($SLFO_4$)	*I*4*mm*	Tetragonal	XRD	0.93 W/cm^2 at 900°C–700°C	–	[136]
$Sr_{2-x}Ba_xMMoO_{6-\delta}$ (M = Co, Ni; x = 0, 0.5, 1.0, 1.5, 2.0)	*Fm*-3*m* ($Sr_2CoMoO_{6-\delta}$) and *I*4/*m*($Sr_2NiMoO_{6-\delta}$)	Cubic ($Sr_2CoMoO_{6-\delta}$) and Tetragonal ($Sr_2NiMoO_{6-\delta}$)	XRD	0.1 W/cm^2 for Co-containing materials and 0.16 W/cm^2 for Ni-containing materials at 850°C	0.2 S/cm for Co-containing materials and $< 10^{-2}$ S/cm for Ni-containing materials at 800°C	[129]
$Sr_2MgMo_{1-x}V_xO_{6-\delta}$ (x = 0–0.2)	–	–	XRD	–	For x = 0.5, 7.71 S/cm at 727°C in 5% H_2/Ar	[137]
$Sr_2Ti_{2x}Ni_{1-x}Mo_{1-x}O_6$ (x = 0, 0.1, 0.3, 0.5, 0.7)	–	–	XRD	–	17–20 S/cm at 600°C–800°C	[138]
$Sr_2Mg(Mo_{0.8}Nb_{0.2})O_{6-\delta}$	–	–	XRD	–	0.2 S/cm at 800°C	[139]
Ba_2MMoO_6 (M = Fe, Co, Mn, Ni)	*Fm*-3*m*	Cubic	XRD	605 mW/cm^2 in H_2 at 850°C	196 S/cm in dry H_2 at 850°C	[140]
$Sr_2MgMoO_{6-\delta}$	*I*4/*m* and $I\bar{4}$at RT and *Fm*-3*m* at 500°C	Tetragonal and triclinic at RT, cubic at 500°C	XRD	–	–	[141]
$Sr_2Fe_{1.5}Mo_{0.5}O_{6-\delta}Gd_{0.1}Ce_{0.9}O_{2-\delta}$ (SFM-GDC)	–	–	XRD	445 mW/cm^2 at 700°C	–	[142]
$Sr_2MgMoO_{6-\delta}$ (SMM) and $Ce_{0.9}Gd_{0.1}O_2$ (GDC)	–	–	XRD	110 mW/cm^2 at 1100°C	–	[143]
$Sr_{2-x}Sm_xMgMoO_{6-\delta}$ (SSMM, $0 \leqslant x \leqslant 0.8$)	*I*4/*m*	Tetragonal	XRD	907 mW/cm^2 at 850°C	For x = 0.6, 16 S/cm in H_2 at 800°C	[27]
$Sr_2Fe_{2-x}Mo_xO_{6-\delta}$ (SFMO)	–	Cubic	XRD	387 mW/cm^2 at 1023 K and 541 mW/cm^2 at 1073 K with H_2, 341 mW/cm^2 at 1023 K and 415 mW/cm^2 at 1073 K with methanol	< 0.1 S/cm in testing condition	[144]

(*Continued*)

Double perovskite anode materials	Space group	Phase	Diffraction pattern	Power density	Conductivity	Ref.
$A_2FeMoO_{6-\delta}$ (A = Ca, Sr, Ba)	$P2_1/n$($Ca_2FeMoO_{6-\delta}$), $I4/m$($Sr_2FeMoO_{6-\delta}$), $Fd-3m$ ($Ba_2FeMoO_{6-\delta}$)	Monoclinic ($Ca_2FeMoO_{6-\delta}$), Tetragonal ($Sr_2FeMoO_{6-\delta}$), Cubic ($Ba_2FeMoO_{6-\delta}$)	XRD	831 mW/cm^2 for A = Sr, 561 mW/cm^2 for A = Ba and 186 mW/cm^2 for A = Ca at 850°C	–	[145]
$Sr_{2-x}MgMoO_{6-\delta}$ (x = 0–0.15)	I-1	Triclinic	XRD	659 mW/cm^2 for x = 0.10 at 800°C	15.7 S/cm at 800°C in H_2	[146]
$Sr_2MgMoO_{6-\delta}$	–	–	XRD	330 mW/cm^2 at 800°C	0.8 S/cm in 5%H_2/Ar at 800°C	[147]
A_2MgMoO_6(A = Sr,Ba)	$P2$ (SMMO) and $P1$ (BMMO)	Monoclinic (SMMO) and triclinic (BMMO)	XRD	–	–	[148]
$Sr_2CoMoO_{6-\delta}$	–	Tetragonal	XRD	1017 mW/cm^2 in H_2 at 800°C	–	[149]
$Sr_2MgMoO_{6-\delta}$	I-1	Triclinic	XRD	–	2.13 S/cm at 800°C	[150]
$Sr_2Mg_{1-x}Al_xMoO_{6-\delta}$ ($0 \leqslant x \leqslant 0.05$)	–	–	XRD	187 mW/cm^2 at 800°C in H_2	5.4 S/cm at 800°C	[77]
$Sr_2Fe_{1.5}Mo_{0.5}O_{6-\delta}$ (SFM)	Pm-3m	Cubic	XRD	–	–	[151]
$Sr_2Fe_{1-x}Ti_xNbO_{6-\delta}$ (x = 0, 0.05, 0.10)	$I4/m$	Tetragonal	XRD	–	1.17 S/cm for SFTN0.1 at 750°C in 5% H_2/Ar	[152]
La2ZnMnO$_6$	$P2_1/n$	Monoclinic	XRD	155 mW/cm^2 at 650°C	0.054 S/cm at 650°C	[153]
$Sr_2FeTiO_{6-\delta}$	Pm-3m	Cubic	XRD	441 mW/cm^2 NiO–SDC/SDC/SFT at 800°C and 335 mW/cm^2 SFT/SDC/SFT at 800°C	2.83 S/cm at 600°C	[154]
$Ba_2FeMoO_{6-\delta}$	–	Cubic	XRD	–	–	[155]
$Sr_{0.5}Ba_{1.5}CoMoO_{6-\delta}$, $SmBa_{0.5}Sr_{0.5}Co_{1.5}Fe_{0.5}O_{5+\delta}$, $YBaCo_2O_{5+\delta}$, $Sr_{0.5}Ba_{1.5}CoMoO_{6-\delta}$	–	–	–	120 mW/cm^2 at 850°C	–	[156]
$Sr_2Fe_{1.5}Mo_{0.5}O_{6-\delta}$	Fm-3m	Cubic	XRD	42.6 mW/cm^2 at 800°C	59.48 (51.96) S/cm at 800°C in air	[157]
$Sr_2FeMoO_{6-\delta}$	Fm-3m	Cubic	XRD	1066 mW/cm^2 at 800°C	25 S/cm at 800°C	[130]
$GdBaCo_2O_{5+x}$	$Pmmm$ for T < 525°C and $P4/mmm$ at 525°C	Orthorhombic (for T < 525°C) and tetragonal (at 525°C)	XRD	–	> 600 S/cm at 800°C	[158]
$Sr_2FeCo_{0.5}Mo_{0.5}O_{6-\delta}$ (SFCM)	$Fm3m$	Cubic	XRD	45.69 mW/cm^2 at 800°C	–	[159]
$Sr_2Fe_{1.5}Mo_{0.5}O_{6-\delta}$ (SFMO)	–	–	XRD	–	–	[160]

(2) Matched thermal expansion coefficient (TEC) and chemical compatibility with the electrolyte and interconnect materials;

(3) High amount of porosity to allow gaseous oxygen to readily diffuse through the cathode to the cathode/electrolyte interface;

(4) Durability under oxidizing atmosphere during fabrication and operation;

(5) High catalytic activity for the oxygen reduction reaction (ORR);

(6) Low cost.

Table 4 presents the structural and electrochemical parameters to compare the cathode materials investigated. In this case, it is worth noting the large spread of conductivity value of 389 S/cm at 850°C (Table 4, Ref. [168]) and the highest power density value of 1541 mW/cm^2 at 800ºC [169].

5 Challenges to use double perovskite in SOFC

The challenges are mainly posed to double perovskite materials located on the ordering of *B*′- and *B*″ materials. In these materials, a deviation from the primitive cubic unit cell is expected due to the differences in the *A*, *B*, and oxygen ion sizes, together with their electronic, oxidation, and magnetic states. This may ultimately induce a lower crystal symmetry and is easily interpreted using the tolerance factor [232]. The major problem raised in SOFC operation is the durability of anode and cathode for a longtime. These components can be affected by either air or fuels used in the system or the volatile types of fuel cell component [233]. To make a perfect SOFC system, not only the high cell performance but also the stability under high temperature and the tolerance of various elements like sulfur are required [164].

5.1 Mixed ionic and electronic conductivity (MIEC)

Mixed ionic electronic conducting (MIEC) double perovskites are very important for electrochemical systems. They are major components in many devices like SOFCs. However, using nickel in anode has a few flaws e.g., these materials deteriorated easily due to sulfur poisoning, poor redox stability, coking (carbon deposition) and the fact that Ni particles to agglomerate after prolonged operation [234]. Aside from doped-$SrTiO_3$ mixed ionic and electronic conductors (MIECs) [235,236], other MIECs that have been investigated as potential anode materials over the last few years include Sr_2FeNbO_6[237], $PrBaCo_2O_{5+\delta}$(PBCO) [238], $Ln_{1-x}Sr_xCr_{0.5}Mn_{0.5}O_{3-\delta}$ (*Ln* = La and Pr) [239], $La_{0.75}Sr_{0.25}Cr_{0.5}Mn_{0.5-x}M_xO_{3-\delta}$ (*M* = Ga, Ti, Mg) [119,121,236], $Ce_{0.9}Sr_{0.1}VO_x$ (x = 3,4) [240], $Sr_2Fe_{4/3}Mo_{2/3}O_6$[69], $YSr_2Fe_3O_8$[241], $PrSrMn_2O_{5+\delta}$ [1] and Sr_2MnMoO_6perovskites [67,242]. (La,Sr)$CoO_{3-\delta}$ (LSC) have also been studied as cathode [243]. (La,Sr)$MnO_{3-\delta}$ (LSM), (La,Sr)$CoO_{3-\delta}$ (LSC) and $La_{0.6}Sr_{0.4}Co_{0.2}Fe_{0.8}O_{3-\delta}$ (LSCF) show mixed ionic and electronic behavior which is good for SOFC cathode [244].

$(La_{0.75}Sr_{0.25})12xCr_{0.5}Mn_{0.5}O_{3-\delta}$ as complex perovskite has very good performances compared with those of hydrogen to nickel-zirconia cermet and excellent catalytic activity with CH_4 at a high temperature [245]. Nonetheless, the low electrical conductivity (1 S/cm at 1000°C) for this material has also been discovered by Tao et al. [246]. Low tolerance against sulfur species is shown in the fuel. Highly redox and chemical stable materials with a high resistance can demolish sulfur impurities, but the electrocatalytic activity and ionic conductivity require more treatment to get good results [247–249].

5.2 Porosity

Electrode materials in SOFC should exhibit a very good microstructure with a uniform particle size and porosity. Porosity acts on transporting gases to/from the fuel cell electrodes. The use of the porous electrode in SOFC assumes that the effect of microstructural properties such as surface area, volume fraction of the various phases, and irregularity of gas, ionic, and electronictransport paths will be improved. Most anodes are porous cermets (a composite of ceramic and metal), which allow conduction of electrons through the structure [250] as well as a cathode. But the electrolytes are dense materials. The cathode reduces partial oxygen pressure by releasing continuous oxygen [251]. A cross-sectional image of SOFC with YSZ electrolyte is shown in Fig. 10. The electrodes present adequate porosity and probably good contact with the electrolyte for $Sr_2BMoO_{6-\delta}$ (*B* = Mg, Ni, Co) and $Sr_2Fe_{1.5}Mo_{0.5}O_{6-\delta}$ [252].

5.3 Phase composition and crystalline structure determination

The phase composition and crystalline structure are one of the main characterizations to be done for the development of SOFC materials. From the cell parameter, the structure of the crystal can be determined. The cation ionic radii, synthesis process, electronic stability, bond strength, and oxygen occupancy play a very crucial role in the crystalline structure determination [253]. X-ray diffraction is the most common structure determination tool for components in SOFC. More accurate oxygen vacancies and atomic positions can be determined only through neutron diffraction [253]. $NdBaMn_2O_{5+\delta}$ has been tested by *in-situ* neutron diffraction and conductivity measurement which shows very promising performance in SOFC [254]. The *B*-site ordered double perovskite cathode, $Ba_2CoMo_{0.5}Nb_{0.5}O_{6-\delta}$ (BCMN), has also been examined by NPD which belongs to the *Fm*-3*m* space group [255].

For example, the X-ray diffraction (XRD) of

Table 4 Various types of methods, space group, phase, conductivity and highest power density of double perovskite type cathode materials fabricated for SOFC

Double perovskite as cathode	Space group	Phase	Diffraction pattern	Power density	Conductivity	Ref.
$NdBaCo_2O_{5+\delta}$, $PrBaCo_2O_{5+\delta}$, $GdBaCo_2O_{5+\delta}$	*P4/mmm* for NBCO, *Pmmm* for both PBCO and GBCO	Tetragonal (NBCO), Orthorhombic (both PBCO and GBCO)	XRD	–	–	[170]
Pr_2NiMnO_6	$P2_1/n$	Monoclinic	XRD	–	3 S/cm at 800°C	[171]
$NdBaFe_{1.9}Nb_{0.1}O_{5+\delta}$	*Pm*-3*m*	Cubic	XRD	392 mW/cm^2 at 700°C	109 S/cm under air, 101 S/cm under N_2 and 119 S/cm under O_2 at 450°C	[172]
$LaSrCoTiO_{5+\delta}$	–	–	XRD	776 mW/cm^2 at 800°C	24–40 S/cm at 300°C–850°C	[173]
$Pr_{1-x}Ca_xBaCo_2O_{5+\delta}$	*P4/mmm*	Tetragonal	XRD	646.5 mW/cm^2 at 800ºC	> 320 S/cm between 300°C and 850°C in air	[174]
$EBaCo_2O_{5+\delta}$	–	–	–	–	150–900 S/cm for $PrBaCo_2O_{5+\delta}$, 200 to 1000 S/cm for $NdBaCo_2O_{5+\delta}$, 100 and 500 S/cm for $GdBaCo_2O_{5+\delta}$, 250 and 850 S/cm for $SmBa_{0.5}Sr_{0.5}Co_2O_{5+\delta}$ at 600°C	[175]
$NdBaFe_{2-x}Mn_xO_{5+\delta}$	*Pm*-3*m*	Cubic	XRD	453 mW/cm^2 at 700°C	114 S/cm in air at 550°C	[176]
$PrBa_{1-x}Co_2O_{5+\delta}$ ($x = 0$–0.1)	*Pmmm*	Orthorhombic	XRD	–	–	[177]
$SmBaCo_{2-x}Ni_xO_{5+\delta}$ ($SBCN_x$) ($x = 0$–0.5)	*Pmmm*	Orthorhombic	XRD	536 mW/cm^2 at 800°C	857–374 S/cm for SBCN0.2 at 400°C–800°C	[178]
$LnBaCoFeO_{5+\delta}$ (*Ln* = Pr, Nd)	*P4/mmm*	Tetragonal	XRD	749 mW/cm^2 for PBCF and 669 mW/cm^2 for NBCF at 800°C	321 S/cm for PBCF and 114 S/cm for NBCF at 350°C	[179]
$PrBaCo_2O_{5.5}$	–	–	–	–	–	[180]
$PrBaCo_{2-x}Cu_xO_{5+\delta}$	*Pmmm*	Orthorhombic	XRD	–	–	[181]
$PrBaCo_2O_{5+\delta}$ (PBC)	*I4/mmm*	Tetragonal	XRD	–	⩾100 S/cm for all tested temperatures	[182]
$NdBa_{0.5}Sr_{0.5}Co_{1.5}Fe_{0.5}O_{5+\delta}$	*Pmmm*	Orthorhombic	XRD	1.02 W/cm^2	–	[182]
$NdBaCo_{2/3}F_{2/3}Cu_{2/3}O_{5+\delta}$ (NBCFC)	*P4/mmm*	Tetragonal	XRD	736 mW/cm^2 at 800°C	92 S/cm at 625°C	[183]
$GdBaFeNiO_{5+\delta}$ (GBFN)	*P4/mmm*	Tetragonal	XRD	515 mW/cm^2 at 800°C	–	[184]
$EuBa_{1-x}Co_2O_{6-\delta}$ ($x = 0$, 0.02, 0.04)	*Pmmm*	Orthorhombic	XRD	505 mW/cm^2 at 700°C	> 150 S/cm	[185]

(*Continued*)

Double perovskite as cathode	Space group	Phase	Diffraction pattern	Power density	Conductivity	Ref.
$PrBaCo_{2/3}Fe_{2/3}Cu_{2/3}O_{5+\delta}$ (PBCFC)	*P4/mmm*	Tetragonal	XRD	659 mW/cm^2 at 800°C	144–113 S/cm between 600°C and 800°C	[186]
$Pr_{0.94}BaCo_2O_{6-\delta}$	*Pmmm*	Orthorhombic	XRD	1.05 W/cm^2 at 600°C	400 S/cm at 100°C–750°C	[187]
Ln$BaCoFeO_{5+\delta}$ (P(N)BCF, (*Ln* = Pr, Nd)	*P4/mmm*	Tetragonal	XRD	960 mW/cm^2 for PBCF–40SDC and 892 mW/cm^2 for NBCF–30SDC at 800°C	92 S/cm for PBCF–40SDC and 107 S/cm for NBCF–30SDC at 375°C	[188]
$YBaCo_{2-x}Fe_xO_{5+\delta}$ (x = 0, 0.2, 0.4, 0.6)	–	Orthorhombic	XRD	For x = 0,873 mW/cm^2 at 800°C	For x = 0, > 300 S/cm at 325°C	[189]
$SmBaCo_2O_{5+x}$ (SBCO)	–	–	XRD	777 mW/cm^2 at 800°C	815–434 S/cm in 500°C–800°C	[190]
$NdBaCu_2O_{5+\delta}$ (NBCO), $NdBa_{0.5}Sr_{0.5}Cu_2O_{5+\delta}$ (NBSCO)	–	–	XRD	–	16.87 S/cm and 51.92 S/cm at 560°C and 545°C	[191]
$SmBaCo_2O_{5+\delta}$ (SBCO)	–	–	XRD	–	–	[192]
$YBa_{0.5}Sr_{0.5}Co_{1.4}Cu_{0.6}O_{5+\delta}$ (YBSCC)	–	Orthorhombic	XRD	398 mW/cm^2 at 850°C	174 S/cm at 350°C in air	[193]
$GdBa_{0.5}Sr_{0.5}Co_{2-x}Fe_xO_{5+\delta}$ ($0 \leqslant x \leqslant 2$)	*P4/mmm* (No. 123)	Tetragonal	XRD	0.25 W/cm^2 at 800°C	1000 S/cm at 400°C	[194]
$SmBaCo_2O_{5+\delta}$	*P4/mmm*	Tetragonal	XRD	304 mW/cm^2 at 700°C	–	[195]
$Y_{0.8}Ca_{0.2}BaCoFeO_{5+\delta}$ (YCBCF)	–	–	XRD	426 mW/cm^2 at 650 °C	–	[196]
$NdBa_{1-x}Co_2O_{5+\delta}$	*Pmmm*orNBC0, NBC5 (*Pmmm*), NBC10 (*P4/mmm*)	Orthorhombic(NBC0), Orthorhombic(NBC5), Tetragonal (NBC10)	XRD	–	–	[197]
Ln$BaCo_{1.6}Ni_{0.4}O_{5+\delta}$(*Ln* = Pr, Nd,Sm)	*P4/mmm* (for PrBCN and NdBCN), *Pmmm* (for SmBCN)	Tetragonal (for PrBCN and NdBCN), Orthorhombic (for SmBCN)	XRD	732, 714, and 572 mW/cm^2 for *Ln* = Pr, Nd, Sm at 800°C	> 235 S/cm between 300°C and 850°C	[198]
$La_{2-x}Sr_xCoTiO_6$ ($0.6 \leqslant x \leqslant 1.0$)	*R*-3*c*	Rhombohedral	XRD	–	13.23 S/cm at 800°C	[199]
$SmBa_{1-x}Ca_xCoCuO_{5+\delta}$ (x = 0–0.3)	–	–	XRD	939 mW/cm^2 at 800°C	–	[200]
$SrCo_{1-x}M_xO_{3-\delta}$ (*M* = Ti, V)	*P4/mmm*	Tetragonal	XRD and NPD	824 mW/cm^2 for M^{n+}= Ti^{4+} (x = 0.05) and 550 mW/cm^2 for M^{n+}= V^{5+} (x = 0.03) at 850°C	above 80 S/cm for M^{n+}= Ti^{4+} and $^{+}$8 S/cm for M^{n+}= V^5 at 850°C	[201]
$SmBaCuCoO_{5+\delta}$	–	Orthorhombic	XRD	355 mW/cm^2 at 700°C	–	[202]
$LaBa_{1-x}Co_2O_{5+\delta}$ (x = 0–0.15)	*P4/mmm*	Tetragonal	XRD	–	280 S/cm between 150°C–850°C	[203]

(*Continued*)

Double perovskite as cathode	Space group	Phase	Diffraction pattern	Power density	Conductivity	Ref.
$Sr_{2-x}Ba_xFe_{1.5}Mo_{0.5}O_{6-\delta}$ (x = 0,0.2,0.4,0.6, 0.8, 1.0)	–	Cubic	XRD	1.63 W/cm^2 800°C	21.7 S/cm at 550°C	[204]
$GdBaCo_{2-x}Fe_xO_{6-\delta}$ (x = 0,0.2)	–	–	XRD	–	450 S/cm at 400°C	[205]
$LaSrMnCoO_{5+\delta}$ (LSMC)	–	Cubic	XRD	565 mW/cm^2 at 800°C	140 S/cm at 850°C	[206]
$Sm_{1-x}BaCo_2O_{5+\delta}$ (x = 0 – 0.08)	*Pmmm*	Orthorhombic	XRD	–	333 S/cm for x = 0.05 at 800°C	[207]
$Sr_2Fe_{1.4}Co_{0.1}Mo_{0.5}O_{6-\delta}$	–	Cubic	XRD	1.16 W/cm^2 at 800°C	28 S/cm at 500°C	[208]
$PrBa_{0.92}CoCuO_{6-\delta}$	*Pmmm*	Orthorhombic	XRD	1541 mW/cm^2 at 800°C	134 S/cm at 800°C in air	[169]
$LnBaCo_2O_{5+\delta}$ (Ln = La, Pr, Nd, Sm, Gd, Y)	*Pmmm*	Orthorhombic	XRD	–	120–350 S/cm, ~180°C in air and 50 to 100 S/cm at ~350°C in N_2	[209]
$La_{2-x}Sr_xCoTiO_6$	$P2_1/n$ (La_2CoTiO_6) and *Pnma* ($La_{1.50}Sr_{0.50}CoTiO_6$)	Monoclinic (La_2CoTiO_6) and orthorhombic ($La_{1.50}Sr_{0.50}CoTiO_6$)	NPD	–	–	[210]
$PrBa_{0.5}Sr_{0.5}CoCuO_{5+\delta}$ (PBSCCO)	–	–	XRD	521 mW/cm^2 at 800°C	483 S/cm at 325°C	[211]
$Nd_{1-x}BaCo_2O_{6-\delta}$	*Pmmm*	Orthorhombic	XRD	370 S/cm	0.6 W/cm^2 at 700°C	[212]
$Sr_2FeTi_{0.75}Mo_{0.25}O_{6-\delta}$ (SFTM)	*Pm3m*	Cubic	XRD	2.31 S/cm at 500°C	394 mW/cm^2 at 800°C	[213]
$YBa_{0.5}Sr_{0.5}Co_2O_{5+\delta}$ (YBSC)	–	–	XRD	650 mW/cm^2 at 850°C	668 S/cm at 325°C	[214]
$SmSrCo_{2-x}Mn_xO_{5+\delta}$ (SSCM, x = 0, 0.2, 0.4, 0.6, 0.8, 1.0)	*Pbnm*	Orthorhombic	XRD	–	1000 S/cm for x = 0	[215]
$PrBa_{0.5}Sr_{0.5}Co_2O_{5+x}$(PBSC)	–	–	XRD	1021 mW/cm^2 at 800°C	581 S/cm at 850°C	[216]
$GdBaCo_{2/3}Fe_{2/3}Cu_{2/3}O_{5+\delta}$	*Pmmm*	Orthorhombic	XRD	800 mW/cm^2 at 800°C	–	[217]
$PrBaCo_{2-x}Sc_xO_{6-\delta}$ (PBCS, x = 0–1.0)	*P4/mmm* (for x = 0–0.2), *Pm-3m* (for x = 0.3–0.9)	Tetragonal (for x = 0–0.2), cubic (for x = 0.3–0.9)	XRD	–	140 S/cm for x = 0.50 at 800°C	[218]
$PrBaCo_{2-x}Fe_xO_{5+\delta}$ (PBCF, x = 0,0.5,1.0)	–	–	XRD	0.70 W/cm^2 at 700°C	> 3 S/cm at 750°C	[219]
$PrBaCo_2O_{5+\delta}$ (PBCO)	–	Orthorhombic	XRD	866 mW/cm^2 at 650°C	–	[220]
$GdBaCo_2O_{5+x}$ (GBCO)	*Pmmm*	Orthorhombic	XRD	500 mW/cm^2 at 800°C	> 30 S/cm at 750°C	[221]
$SmBa_{0.5}Sr_{0.5}Co_2O_{5+\delta}$ (SBSC)	–	Fluorite	XRD	1147 mW/cm^2 at 700°C	–	[222]
$Sr_2Fe_{1.5}Mo_{0.5}O_{6-\delta}$ (SFM)	*Pnma*	Orthorhombic	XRD	1102 mW/cm^2 at 800°C	~30 S/cm at 550°C	[223]

(*Continued*)

Double perovskite as cathode	Space group	Phase	Diffraction pattern	Power density	Conductivity	Ref.
$NdBa_{0.5}Sr_{0.5}Co_2O_{5+x}$	–	Orthorhombic	XRD	904 m/cm^2 at 850°C	1368 S/cm at 100°C and 398 S/cm at 850°C	[168]
$Pr_{0.83}BaCo_{1.33}Sc_{0.5}O_{6-\delta}$–0.17$PrCoO_3$ (PBCS-0.17PCO)	*Pm*-3*m*	Cubic	XRD	–	18 S/cm in 100°C–750°C	[224]
$PrBaCo_{2-x}Fe_xO_{5+\delta}$ ($0 \leqslant x \leqslant 2$)	*P4/mmm* (for $x = 0$, 0.2), *Pm*-3*m* (for $x = 0.4,0.6,0.8,1.0,2.0$)	Tetragonal (for $x = 0$, 0.2), cubic (for $x = 0.4$, 0.6,0.8,1.0,2.0)	XRD	446.4 mW/cm^2 for PBCF0.4 at 700°C	457.2 S/cm for PBCF0.4	[225]
$YBaCo_{2-x}Cu_xO_{5+\delta}$ ($x = 0$, 0.2,0.4,0.6,0.8)	–	Tetragonal	XRD	816 mW/cm^2 for $x = 0.6$ at 850°C	43 S/cm for $x = 0.01$ at 300°C	[226]
$SmBaCoCuO_{5+x}$ (SBCCO)	–	Orthorhombic	XRD	517 mW/cm^2 at 800°C	34 S/cm at 850°C	[227]
Ln$Ba_{0.5}Sr_{0.5}Co_2O_{5+\delta}$ (*Ln* = Pr, Nd)	*P4/mmm*	Tetragonal	XRD	–	240 S/cm and 131 S/cm in the temperature range (80°C–900°C)	[228]
$GdBaCo_{2-x}Ni_xO_{5+\delta}$ (x = 0–0.8, cathode)	*Pmmm*	Orthorhombic	XRD	–		[229]
$PrBa_{0.5}Sr_{0.5}Co_{2-x}Fe_xO_{5+\delta}$ (PBSCF, x = 0.5, 1.0, 1.5)	*Pmmm*	Orthorhombic	XRD	97 mW/cm^2 for $x = 0.56$ at 850°C	60–769 S/cm in 250°C–850°C	[229]
$Sr_2Fe_{1-x}Co_xNbO_6$ (SFCN, $0.1 \leqslant x \leqslant 0.9$)	–	Tetragonal	XRD	–	5.7 S/cm for SFCN09 at 800°C	[230]
$SmBa_{0.6}Sr_{0.4}Co_2O_{5+\delta}$	*P4/mmm*	Tetragonal	XRD	–	–	[231]

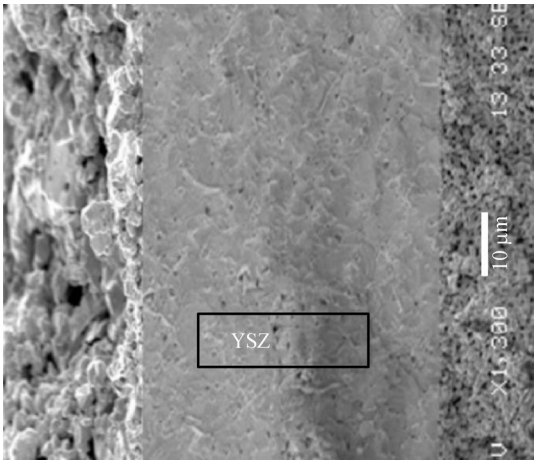

Fig. 10 Cross-sectional SEM micrographs of the SOFC microstructure (adapted with permission from Ref. [21]).

$A_2FeMoO_{6-\delta}$ samples in 5% H_2/Ar for 10 h are shown in Fig. 11 where the sintering temperature is 1100°C. The single-phase double perovskite oxides $A_2FeMoO_{6-\delta}$ has been observed after final sintering. The XRD pattern shows a clear observation with zero impurity. $Ca_2FeMoO_{6-\delta}$ exhibits a monoclinic structure with the space group $P2_1/n$, $Sr_2FeMoO_{6-\delta}$ shows a tetragonal structure with the $I4/m$ space group, and $Ba_2FeMoO_{6-\delta}$ manifests a cubic structure with the Fm-3m space group. Besides, $NdSrMn_2O_6$ can be a good anode with an orthorhombic ($Pmmm$) structure [256]. These are appropriately fitted with the given materials [257,258]. Figure 11 shows the Rietveld refinement profile of a new anode material which has been reported recently.

5.4 Electrical conductivity

The electronic conductivity of double perovskite materials depends mainly on the *B*-site cation ordering. Almost all the transitional metals, lanthanides, and actinides can occupy in the *B*-site. Mostly, the elements occupy in the periodic table 3*d*, 4*d*, or 5*d* series show very alluring electrical conductive properties. Most of the DP elements show insulating or semiconducting behavior as described in the literature. The real challenge is to identify a good stable electrode material exhibiting a high conductivity in a reduced atmosphere for SOFC operation.

Zhang and He [27] have measured the electrical conductivity of $Sr_{2-x}Sm_xMgMoO_{6-\delta}$ by using the van der Pauw method running under H_2 at different temperatures. The highest value of conductivity is found at $x = 0.6$ and it is 16 S/cm in H_2 at 800°C [260]. The electrical conductivity of SSMM samples in H_2, measured during the time of cooling is shown in Fig. 12. The polaronic conducting behavior is commonly seen for these samples running in H_2. As molybdenum is a very good catalyst, these samples demonstrate that the amount of Mo increases with supplanting Sm instead of Sr.

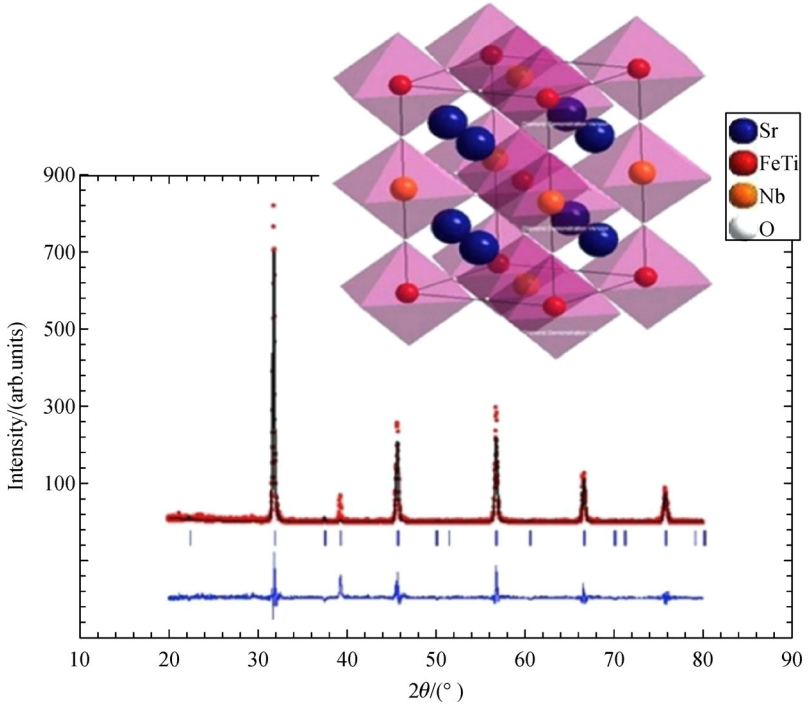

Fig. 11 Observed (red dots) and calculated (black line) XRD intensity profiles for SFTN0.05 at room temperature (The short vertical lines indicate the angular position of the allowed Bragg reflections. At the bottom, the difference plot (blue line), I_{obs}–I_{calc}, is shown. Insert shows the 3D schematic diagram, adapted with permission from Ref. [259].)

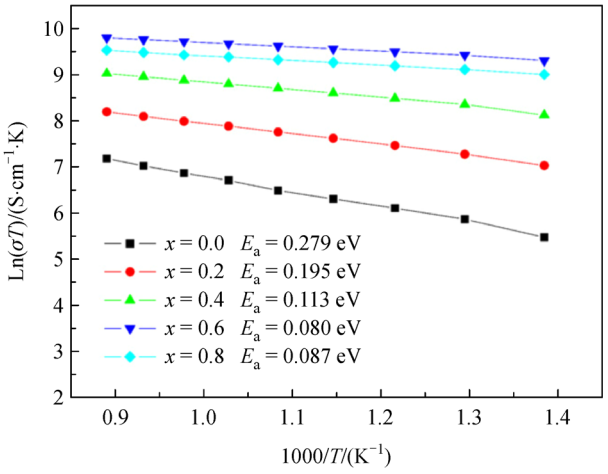

Fig. 12 Electrical conductivity of the SSMM sample ($0 \leqslant x \leqslant 0.8$) sintered at 1200 °C for 20 h (adapted with permission from Ref. [27]).

In all atmospheres, a positive temperature coefficient is observed from Fig. 12, i.e., the polaron helps to increase the value of conductivity with increasing temperature. In air, σ which is temperature dependence can be discussed with the whole temperature range $400°C \leqslant T \leqslant 800°C$ by polaron expression $\sigma = (A/T)\exp(-E_a/kT)$, where the activation energy $E_a = \Delta H_m + \Delta H_t/2$ is the sum of the polaron motional enthalpy ΔH_m and the enthalpy ΔH_t to free a polaron from the oxygen vacancy that creates it. The value of E_a is (0.134±0.001) eV. In 5% H_2/Ar, the formation of oxygen vacancies with the introduction of additional electronic polaron charge carriers leads to a reduction.

In consonance with Zhang et al. [145] on $A_2FeMoO_{6-\delta}$ (A = Ca, Sr, Ba), the bulk electrical resistivity is acting as a function of temperature for the samples $A_2FeMoO_{6-\delta}$ in H_2 between the temperature range of 50°C and 850°C. For $Ca_2FeMoO_{6-\delta}$, the electrical resistivity is suggested that metallic-like conduction behavior is seen throughout the whole measured temperature range. The electrical resistivity of $Sr_2FeMoO_{6-\delta}$, in another way, can be described for various conduction behaviors in three regions:

(1) Metallic conduction behavior below 150°C;

(2) Semiconducting region or localization of the carriers in the temperature range of 150°C–550°C;

(3) Reverting to metallic conduction behavior between 550°C and 850°C.

5.5 Fuel cell performance

The performance of fuel cells depends mainly on constituent materials, their processing, and microstructure.

A number of researches have been conducted to measure single-cell performances using different types of materials, fuels at different temperatures. A good performance of SOFC also means a very attractive material for that cell. All studies have been listed in Tables 2 and 3 where double perovskites have been used as anode or cathode.

$Sr_{2-x}Sm_xMgMoO_{6-\delta}$ (726 mW/cm^2) (SSMM) [260], $Sr_2CoMoO_{6-\delta}$ (1017 mW/cm^2) (SCMO) [68] and $A_2FeMoO_{6-\delta}$ (A = Ca, Sr, Ba) (831 mW/cm^2) [261] are some examples of double perovskite electrodes showing good performance. The $Sr_2CoMoO_{6-\delta}$ anode material has been prepared and assessed for single fuel cell running on H_2 and CH_4 fuels to appraise its electrochemical performance. 300 μm-thick LSGM electrolyte has been assembled to test the cell, and a thin LDC buffer layer between the electrolyte and anode has been used with a porous SFC cathode, like, SCMO/LDC/LSGM/SCF combination. The power density as a function of current density at 800°C as well as cell voltage is featured in Fig. 13. $Sr_2CoMoO_{6-\delta}$ anode manifests an excellent performance under H_2 and wet CH_4 (containing 3% H_2O). The maximum power density P_{max} is 1017 mW/cm^2 under H_2, and 634 mW/cm^2 under wet CH_4at 800°C for $Sr_2CoMoO_{6-\delta}$, and the values are significantly higher than those with of $Sr_2MgMoO_{6-\delta}$ anode [67].

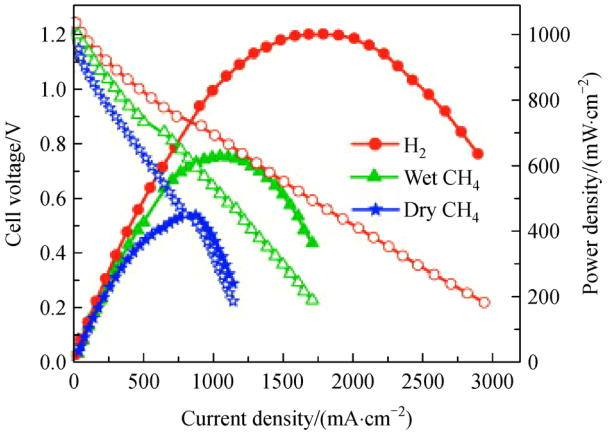

Fig. 13 Power density and cell voltage as functions of current density in H_2, dry CH_4 and wet CH_4 at 800 °C for $Sr_2CoMoO_{6-\delta}$ (adapted with permission from Ref. [68]).

Consequently, the high performance for $Sr_2CoMoO_{6-\delta}$ in wet CH_4 fuel is resulted from the reformer reaction (5) that not only abolishes the CO resulting from reaction (2) but also releases H_2 to create the extra oxide-ion vacancies.

6 Conclusions

SOFCs made with the perovskite oxide materials have definitely increased the interest over the last 20 years. The vast diversity of compositions obtained with doping elements allows the modification of properties in a wide range. Higher efficiencies and electricity generation

enhances the chance to use SOFC in day-to-day life and make it the most auspicious candidate of the renewable energy sector.

Based on the literature, it has been found that double perovskite materials perform as the most amicable materials that can be used as an electrode in SOFC for its impressive catalytic traits. The structural and electrochemical properties are generally determined by the arrangement of the *B*-site cations. Ordering and disordering of *B*-site cations play a vital role in making a suitable electrode for SOFC.

Researchers have already worked on making high-performance electrode with perovskite. Synthesizing, oxidation state, and the *B*-site cation ordering are mainly responsible for achieving maximum power density as they show good carbon and sulfur tolerance in commercial city gas.

There are different compositions with a wide range of properties of double perovskite materials that can be synthesized. Novel materials for SOFC still attract researchers to create a new podium in the transport and industrial sector. To make a cost-effective, high catalytically active electrode operated at low temperature for SOFC will be the next step.

7 Recommendation for future work

In the SOFC sector, many experiments have been done to produce a much more effective and inexpensive cell that can be used in day to day life easily. Though double perovskites electrode materials have been used already in practical sectors, it is still a distant dream. The current research has focused on the development of double perovskite electrodes that can be used in SOFC because researchers have not yet obtained the practically stable double perovskite electrode materials which can be used economically in commercial sectors.

Future research needs to focus on finding more efficient anodes for direct hydrocarbon conversion that are sulfur tolerant and can be operated at a relatively low temperature. These materials should have a good electrical conductivity as well as a good stablity at a high temperature. SOFC is a device with a solid-solid and gas-solid interface that should be stable at an exalted temperature for a long time. The double perovskite structure can accommodate different types of combinations of transition metals and lanthanides. Because of the potential of the perovskite structure to tolerate a wide range of elements of different sizes and charges, there is a large number of possible permutations of these cations. There are nine possible open d^n configurations, giving $(9\times8)/2$ distinct pairs of $3d$ ions. However, $4d$ ions are also likely to be magnetic in these compounds, including the number of possibilities of $(18\times17)/2$ pairs. Since an ion can be in a few different charge states, each $3d^n$ or $4d^n$ configuration can be attained by more than one ion. If an average of two charge states per ion are taken, another factor of 2^2 can be obtained. The cation A can be chosen from di- and tri-valent cations (including the rare earth) and even some univalent ions, amounting to some 25 ions. The number of compounds then is of the order of

$$25 \times 2^2 \times \frac{18 \times 17}{2} \approx 15000. \quad (7)$$

Considering also the possibility of splitting the cation A to $A'A''$ leads to an additional factor of 24/2 or a total of the order of 2×10^5 [262]. This perspective can facilitate the design of the next generation SOFC using double perovskite electrode materials for finding practical application in power generation.

Acknowledgements The University Graduate Scholarship (UGS) of Universiti Brunei Darussalam is gratefully acknowledged. This work was supported by the project No. UBD/RSCH/URC/RG(6)2018/002.

References

1. Sengodan S, Choi S, Jun A, Shin T H, Ju Y W, Jeong H Y, Shin J, Irvine J T S, Kim G. Layered oxygen-deficient double perovskite as an efficient and stable anode for direct hydrocarbon solid oxide fuel cells. Nature Materials, 2015, 14(2): 205–209
2. Andújar J M, Segura F. Fuel cells: history and updating. A walk along two centuries. Renewable & Sustainable Energy Reviews, 2009, 13(9): 2309–2322
3. Abdalla A M, Hossain S, Petra P M, Ghasemi M, Azad A K. Achievements and trends of solid oxide fuel cells in clean energy field: a perspective review. Frontiers in Energy, 2018, 12(1): 1–24
4. Abdalla A M, Hossain S, Nisfindy O B, Azad A T, Dawood M, Azad A K. Hydrogen production, storage, transportation and key challenges with applications: a review. Energy Conversion and Management, 2018, 165: 602–627
5. Wang S, Jiang S P. Prospects of fuel cell technologies. National Science Review, 2017, 4(2): 163–166
6. Garche J, Ju rissen L. Applications of fuel cell technology: status and perspectives. Electrochemical Society Interface, 2015, 24(2): 39–43
7. U.S. Department of Energy. Fuel cell technologies office. 2015, available at energy.gov website
8. Johnson Matthey P L C. Fuel cell applications–fuel cell today. 2018-11-22, available at fuelcelltoday.com webite
9. Financial Times. Japan is betting future cars will use hydrogen fuel cells. 2018-03-27, available at ft.com website
10. Nissan Motor Corporation. Runnig on e-Bio: Nissan's solid oxide fuel cell system. 2016-06-14, available at nissan-global.com website
11. INSIDEEVS. Navigant: fuel cell vehicle sales to exceed 228000 units by 2024. 2015-12-27, available at insideevs.com website
12. Ang S M C, Fraga E S, Brandon N P, Samsatli N J, Brett D J L. Fuel cell systems optimisation–methods and strategies. International Journal of Hydrogen Energy, 2011, 36(22): 14678–14703

13. Stambouli A B, Traversa E, Stambouli A. Solid oxide fuel cells (SOFCs): a review of an environmentally clean and efficient source of energy. Renewable & Sustainable Energy Reviews, 2002, 6(5): 433–455
14. Laosiripojana N, Wiyaratn W, Kiatkittipong W, Arpornwichanop A, Soottitantawat A, Assabumrungrat S. Reviews on solid oxide fuel cell technology. Engineering Journal (New York), 2009, 13(1): 65–84
15. Minh N Q. Solid oxide fuel cell technology-features and applications. Solid State Ionics, 2004, 174(1-4): 271–277
16. Bao C, Wang Y, Feng D L, Jiang Z, Zhang X. Macroscopic modeling of solid oxide fuel cell (SOFC) and model-based control of SOFC and gas turbine hybrid system. Progress in Energy and Combustion Science, 2018, 66: 83–140
17. Rits V, Kypreos S, Wokaun A. Evaluating the diffusion of fuel-cell cars in the China markets. IATSS Research, 2004, 28(1): 34–46
18. Venture Radar. SOFC | Venture Radar Search. 2018, available at ventureradar.com website
19. Business Wire.Top emerging trends in the global solid oxide fuel cell market| Technavio. 2018-04-04, available at businesswire.com website
20. Markets and Markets. Solid oxide fuel cell market by type (planar and tubular), application (power generation, combined heat & power, and military), end-use (data centers, commercial & retail, and APU), region (north America, Asia Pacific, and Europe)–global forecast to 2025. 2017, available at marketsandmarkets.com website
21. Abdalla A M, Hossain S, Zhou J, Petra P M I, Erikson S, Savaniu C D, Irvine J T S, Azad A K. $NdBaMn_2O_{5+\delta}$ layered perovskite as an active cathode material for solid oxide fuel cells. Ceramics International, 2017, 43(17): 15932–15938
22. Taroco H A, Santos J A F, Domingues R Z, Matencio T. Ceramic materials for solid oxide fuel cells. 2011, available at intechopen.com website
23. Sengodan S, Choi S, Jun A, Shin T H, Ju Y W, Jeong H Y, Shin J, Irvine J T S, Kim G. Layered oxygen-deficient double perovskite as an efficient and stable anode for direct hydrocarbon solid oxide fuel cells. Nature Materials, 2015, 14(2): 205–209
24. Liu Q, Dong X, Xiao G, Zhao F, Chen F. A Novel electrode material for symmetrical SOFCs. Advanced Materials, 2010, 22(48): 5478–5482
25. Huang Y H. Double perovskites as anode materials for solid-oxide fuel cells. Science, 2006, 312(5771): 254–257
26. Atkinson A, Barnett S, Gorte R J, Irvine J T S, McEvoy A J, Mogensen M, Singhal S C, Vohs J. Advanced anodes for high-temperature fuel cells. Nature Materials, 2004, 3(1): 17–27
27. Zhang L, He T. Performance of double-perovskite $Sr_{2-x}Sm_xMgMoO_{6-\delta}$ as solid-oxide fuel-cell anodes. Journal of Power Sources, 2011, 196(20): 8352–8359
28. Steele B C, Heinzel A. Materials for fuel-cell technologies. Nature, 2001, 414(6861): 345–352
29. Singhal S C. Solid oxide fuel cells for stationary, mobile, and military applications. Solid State Ionics, 2002, 152–153: 405–410
30. Shao Z, Haile S M. A high-performance cathode for the next generation of solid-oxide fuel cells. Nature, 2004, 431(7005): 170–173
31. Han D, Liu X, Zeng F, Qian J, Wu T, Zhan Z. A micro-nano porous oxide hybrid for efficient oxygen reduction in reduced-temperature solid oxide fuel cells. Scientific Reports, 2012, 2(1): 462
32. Murray E P, Tsai T, Barnett S A. A direct-methane fuel cell with a ceria-based anode. Nature, 1999, 400(6745): 649–651
33. Park S, Vohs J, Gorte R. Direct oxidation of hydrocarbons in a solid-oxide fuel cell. Nature, 2000, 404(6775): 265–267
34. McIntosh S, Gorte R J. Direct hydrocarbon solid oxide fuel cells. Chemical Reviews, 2004, 104(10): 4845–4866
35. Abdalla A M, Hossain S, Azad A T, Petra P M I, Begum F, Eriksson S G, Azad A K. Nanomaterials for solid oxide fuel cells: a review. Renewable & Sustainable Energy Reviews, 2018, 82: 353–368
36. Safran. Fuel cells: green energy on board. 2018-11-22, available at safran-group.com website
37. Reza M S, Ahmed A, Caesarendra W, Abu Bakar M S, Shams S, Saidur R, Aslfattahi N, Azad A K. Acacia holosericea: an invasive species for bio-char, bio-oil, and biogas production. Bioengineering Multidisciplinary Digital Publishing Institute, 2019, 6(2): 33
38. Justin Fitzgerald and Nancy O'Bryan. NASA– Fuel cells: a better energy source for earth and space. 2005-11-02, available at nasa.gov website
39. Singhal S. Advances in solid oxide fuel cell technology. Solid State Ionics, 2000, 135(1–4): 305–313
40. Tao S W, Irvine J T S. A stable, easily sintered proton-conducting oxide electrolyte for moderate-temperature fuel cells and electrolyzers. Advanced Materials, 2006, 18(12): 1581–1584
41. Radenahmad N, Afif A, Petra P I, Rahman S M H, Eriksson S G, Azad A K. Proton-conducting electrolytes for direct methanol and direct urea fuel cells–a state-of-the-art review. Renewable & Sustainable Energy Reviews, 2016, 57: 1347–1358
42. Malavasi L, Fisher C A J, Islam M S. Oxide-ion and proton conducting electrolyte materials for clean energy applications: structural and mechanistic features. Chemical Society Reviews, 2010, 39(11): 4370–4387
43. Hossain S, Abdalla A M, Jamain S N B, Zaini J H, Azad A K. A review on proton conducting electrolytes for clean energy and intermediate temperature-solid oxide fuel cells. Renewable & Sustainable Energy Reviews, 2017, 79: 750–764
44. Liu M, Lynch M E, Blinn K, Alamgir F M, Choi Y M. Rational SOFC material design: new advances and tools. Materials Today, 2011, 14(11): 534–546
45. Cologna M. Advances in the production of planar and micro-tubular solid oxide fuel cells. Dissertation for the Doctoral Degree. Trento: University of Trento
46. Stambouli A B, Traversa E. Solid oxide fuel cells (SOFCs): a review of an environmentally clean and efficient source of energy. Renewable & Sustainable Energy Reviews, 2002, 6(5): 433–455
47. Hatchwell C E, Sammes N M, Kendall K. Cathode current-collectors for a novel tubular SOFC design. Journal of Power Sources, 1998, 70(1): 85–90
48. National Energy Technology Laboratory. Solid oxide fuel cell. 2018-11-26, available at netl.doe.gov website
49. Vaillant unveils wall-mounted CHP unit, using staxera SOFC. Fuel Cells Bulletin, 2011, 5: 4
50. Kupecki J. Off-design analysis of a micro-CHP unit with solid

oxide fuel cells fed by DME. International Journal of Hydrogen Energy, 2015, 40(35): 12009–12022
51. SOLID power. For private households–SOLID power. 2018-11-26, available at solidpower.com website
52. Peña M A, Fierro J L G. Chemical structures and performance of perovskite oxides. Chemical Reviews, 2001, 101(7): 1981–2018
53. Cava R J, Batlogg B, Krajewski J J, Farrow R, Rupp L W, White A E, Short K, Peck W F, Kometani T. Superconductivity near 30 K without copper: the $Ba_{0.6}K_{0.4}BiO_3$ perovskite. Nature, 1988, 332 (6167): 814–816
54. Zhang Z, Li J, Zhou W, Yang C, Cao Q, Wang D, Du Y. Mechanism of enhancement in magnetoresistance properties of manganite perovskite ceramics by current annealing. Ceramics International, 2018, 44(4): 3760–3764
55. Afroze S, Binti Haji Bakar A N, Reza M S, Salam M A. Polyvinylidene fluoride (PVDF) piezoelectric energy harvesting from rotary retracting mechanism: imitating forearm motion. IET Conference Publications, 2018
56. Schlom D G, Chen L Q, Pan X, Schmehl A, Zurbuchen M A. A thin film approach to engineering functionality into oxides. Journal of the American Ceramic Society, 2008, 91(8): 2429–2454
57. Locock A J, Mitchell R H. Perovskite classification: an excel spreadsheet to determine and depict end-member proportions for the perovskite- and vapnikite-subgroups of the perovskite supergroup. Computers & Geosciences, 2018, 113: 106–114
58. Li R, Yu C, Shen S. Partial oxidation of methane to syngas using lattice oxygen of $La_{1-x}Sr_xFeO_3$ perovskite oxide catalysts instead of molecular oxygen. Journal of Natural Gas Chemistry, 2002, 11: 137–144
59. El-Ads E. Perovskite nanomaterials–synthesis, characterization, and applications. InTech, 2016: 107–151
60. Azad A K. Synthesis, structure, and magnetic properties of double perovskites of the type A_2MnBO_6 and A_2FeBO_6 (A = Ca, Sr, Ba, La; B = W, Mo, Cr). 2004, available at lib.ugent.be website
61. Azad A K, Mellergård A, Eriksson S G, Ivanov S A, Eriksen J, Rundlöf H. Preparation, crystal and magnetic structure of the double perovskite Ba_2FeWO_6. Applied Physics A: Materials Science & Processing, 2002, 74(Sup.1): s763–s765
62. Azad A, Eriksson S G. Formation of a cubic Sr_2MnWO_6 phase at elevated temperature: a neutron powder diffraction study. Solid State Communications, 2003, 126(9): 503–508
63. Azad A, Eriksson S G, Ivanov S, Mathieu R, Svedlindh P, Eriksen J, Rundlöf H. Synthesis, structural and magnetic characterisation of the double perovskite A_2MnMoO_6 (A = Ba, Sr). Journal of Alloys and Compounds, 2004, 364(1–2): 77–82
64. Azad A K, Ivanov S, Eriksson S G, Rundlöf H, Eriksen J, Mathieu R, Svedlindh P. Structural and magnetic properties of the double perovskite Sr_2MnWO_6. Journal of Magnetism and Magnetic Materials, 2001, 237(2): 124–134
65. Azad A K, Ivanov S A, Eriksson S G, Eriksen J, Rundlöf H, Mathieu R, Svedlindh P. Nuclear and magnetic structure of Ca_2MnWO_6: a neutron powder diffraction study. Materials Research Bulletin, 2001, 36(13–14): 2485–2496
66. Azad A K, Eriksson S G, Ivanov S A, Rundlöf H, Eriksen J, Mathieu R, Svedlindh P. Structural and magnetic characterisation of the double perovskites $AA'MnWO_6$ (AA' = Ba_2, SrBa, Sr_2, SrCa and Ca_2). Ferroelectrics, 2002, 269(1): 105–110
67. Huang Y H, Dass R I, Xing Z L, Goodenough J B. Double perovskites as anode materials for solid-oxide fuel cells. Science, 2006, 312(5771): 254–257
68. Zhang P, Huang Y H, Cheng J G, Mao Z Q, Goodenough J B. Sr_2CoMoO_6 anode for solid oxide fuel cell running on $\{H_2\}$ and $\{CH_4\}$ fuels. Journal of Power Sources, 2011, 196(4): 1738–1743
69. Xiao G, Liu Q, Dong X, Huang K, Chen F. $Sr_2Fe_{4/3}Mo_{2/3}O_6$ as anodes for solid oxide fuel cells. Journal of Power Sources, 2010, 195(24): 8071–8074
70. Marrero-López D, Peña-Martínez J, Ruiz-Morales J C, Pérez-Coll D, Aranda M A G, Núñez P. Synthesis, phase stability and electrical conductivity of $Sr_2MgMoO_{6-\delta}$ anode. Materials Research Bulletin, 2008, 43(8–9): 2441–2450
71. Bernuy-Lopez C, Allix M, Bridges C A, Claridge J B, Rosseinsky M J. $Sr_2MgMoO_{6-\delta}$: structure, phase stability, and cation site order control of reduction. Chemistry of Materials, 2007, 19(5): 1035–1043
72. Vasala S, Lehtimäki M, Huang Y H, Yamauchi H, Goodenough J B, Karppinen M. Degree of order and redox balance in B-site ordered double-perovskite oxides, $Sr_2MMoO_{6-\delta}$ (M = Mg, Mn, Fe, Co, Ni, Zn). Journal of Solid State Chemistry, 2010, 183(5): 1007–1012
73. Azizi F, Kahoul A, Azizi A. Effect of La doping on the electrochemical activity of double perovskite oxide Sr_2FeMoO_6 in alkaline medium. Journal of Alloys and Compounds, 2009, 484 (1–2): 555–560
74. Huang Y H, Dass R I, Denyszyn J C, Goodenough J B. Synthesis and characterization of $Sr_2MgMoO_{6-\delta}$: an anode material for the solid oxide fuel cell. Journal of the Electrochemical Society, 2006, 153(7): A1266–A1272
75. Xie Z, Zhao H, Du Z, Chen T. Effects of Co doping on the electrochemical performance of double perovskite oxide $Sr_2MgMoO_{6-\delta}$ as an anode material for solid oxide fuel cells. Journal of Physical Chemistry, 2012, 116: 9734–9743
76. Pan X, Wang Z, He B, Wang S, Wu X, Xia C. Effect of Co doping on the electrochemical properties of $Sr_2Fe_{1.5}Mo_{0.5}O_6$ electrode for solid oxide fuel cell. International Journal of Hydrogen Energy, 2013, 38(10): 4108–4115
77. Xie Z, Zhao H, Chen T, Zhou X, Du Z. Synthesis and electrical properties of Al-doped $Sr_2MgMoO_{6-\delta}$ as an anode material for solid oxide fuel cells. International Journal of Hydrogen Energy, 2011, 36(12): 7257–7264
78. Goldschmidt V M. Die Gesetze der Krystallochemie. Naturwissenschaften, 1926, 14(21): 477–485
79. Shannon R D. Revised effective ionic radii and systematic studies of interatomie distances in halides and chaleogenides. Acta Crystallographica, 1976, 32(5): 751–767
80. Rebaza A V G, Toro C E D, Téllez D A L, Roa-Rojas J. Electronic structure of the double perovskite $Ba_2Er(Nb,Sb)O_6$. Journal of Physics: Conference Series, 2014, 480: 012041
81. Fu W T, IJdo D J W. X-ray and neutron powder diffraction study of the double perovskites Ba_2LnSbO_6 (Ln = La, Pr, Nd and Sm). Journal of Solid State Chemistry, 2005, 178(7): 2363–2367
82. Gopalakrishnan J, Chattopadhyay A, Ogale SB, Venkatesan T, Greene R L, Millis A J, Ramesha K, Hannoyer B, Marest G.

Metallic and nonmetallic double perovskites: a case study of A_2FeReO_6 (A = Ca, Sr, Ba). 2000, 62(14): 9538–9542

83. Davis M J, Mugavero S J III, Glab K I, Smith M D, zur Loye H C. The crystal growth and characterization of the lanthanide-containing double perovskites Ln_2NaIrO_6 (Ln = La, Pr, Nd). Solid State Sciences, 2004, 6(5): 413–417
84. Yamamura K, Wakeshima M, Hinatsu Y. Structural phase transition and magnetic properties of double perovskites Ba_2CaMO_6 (M = W, Re, Os). Journal of Solid State Chemistry, 2006, 179(3): 605–612
85. Gens R, Fuger J, Morss L R, Williams C W. Thermodynamics of actinide perovskite-type oxides III. Molar enthalpies of formation of B_2MAnO_6 (M = Mg, Ca, or Sr; An = U, Np, or Pu) and M_3PuO_6 (M = Ba or Sr). Journal of Chemical Thermodynamics, 1985, 17 (6): 561–573
86. Fu W T, IJdo D J W. Re-examination of the structure of Ba_2MIrO_6 (M = La, Y): space group revised. Journal of Alloys and Compounds, 2005, 394(1–2): 10–13
87. Bharti C, Sinha T P. Dielectric properties of rare earth double perovskite oxide Sr_2CeSbO_6. Solid State Sciences, 2010, 12(4): 498–502
88. Shaheen R, Bashir J. Ca_2CoNbO_6: a new monoclinically distorted double perovskite. Solid State Sciences, 2010, 12(8): 1496–1499
89. Gemmill W R, Smith M D, zur Loye H C. Synthesis, structural characterization, and magnetic properties of the antiferromagnetic double perovskites Ln_2LiOsO_6 (Ln = La, Pr, Nd, Sm). Journal of Solid State Chemistry, 2006, 179(6): 1750–1756
90. Zhang Y, Ji V. Half-metallic ferromagnetic nature of the double perovskite Pb_2FeMoO_6 from first-principle calculations. Journal of Physics and Chemistry of Solids, 2012, 73(9): 1116–1121
91. Mugavero S J III, Smith M D, zur Loye H C. The crystal growth and magnetic properties of Ln_2LiIrO_6 (Ln = La, Pr, Nd, Sm, Eu). Journal of Solid State Chemistry, 2005, 178(1): 200–206
92. Zhou Q, Kennedy B J, Howard C J, Elcombe M M, Studer A J. Structural phase transitions in $A_{2-x}Sr_xNiWO_6$ (A = Ca or Ba, $0 \leqslant x \leqslant 2$) double perovskites. Chemistry of Materials, 2005, 17 (21): 5357–5365
93. Azad A, Eriksson S G, Ivanov S, Mathieu R, Svedlindh P, Eriksen J, Rundlöf H. Synthesis, structural and magnetic characterisation of the double perovskite A_2MnMoO_6 (A = Ba, Sr). Journal of Alloys and Compounds, 2004, 364(1-2): 77–82
94. Strandbakke R, Cherepanov V A, Zuev A Y, Tsvetkov D S, Argirusis C, Sourkouni G, Prünte S, Norby T. Gd- and Pr-based double perovskite cobaltites as oxygen electrodes for proton ceramic fuel cells and electrolyser cells. Solid State Ionics, 2015, 278: 120–132
95. Philipp J B, Majewski P, Alff L, Erb A, Gross R, Graf T, Brandt M S, Simon J, Walther T, Mader W, Topwal D, Sarma D D. Structural and doping effects in the half-metallic double perovskite A_2CrWO_6. Physical Review. B, 2003, 68(14): 144431
96. Popov G, Greenblatt M, Croft M. Large effects of A-site average cation size on the properties of the double perovskites $Ba_{2-x}Sr_x$ $MnReO_6$: a d^5–d^1 system. Physical Review. B, 2003, 67(2): 024406
97. Westerburg W, Lang O, Ritter C, Felser C, Tremel W, Jakob G. Magnetic and structural properties of the double-perovskite Ca_2FeReO_6. Solid State Communications, 2002, 122(3–4): 201–206
98. Falcón H, Barbero J A, Araujo G, Casaisc M T, Martínez-Lope M J, Alonso J A, Fierro J L G. Double perovskite oxides $A_2FeMoO_{6-\delta}$ (A = Ca, Sr and Ba) as catalysts for methane combustion. Applied Catalysis B: Environmental, 2004, 53(1): 37–45
99. Retuerto M, Alonso J A, García-Hernández M, Martínez-Lope M J. Synthesis, structure and magnetic properties of the new double perovskite Ca_2CrSbO_6. Solid State Communications, 2006, 139 (1): 19–22
100. Hu R, Ding R, Chen J, Hu J, Zhang Y. Preparation and catalytic activities of the novel double perovskite-type oxide La_2CuNiO_6 for methane combustion. Catalysis Communications, 2012, 21: 38–41
101. Peña M A, Fierro J L G. Chemical structures and performance of perovskite oxides. Chemical Reviews, 2001, 101(7): 1981–2018
102. Parfitt D, Chroneos A, Tarancón A, Kilner J A. Oxygen ion diffusion in cation ordered/disordered $GdBaCo_2O_{5+\delta}$. Journal of Materials Chemistry, 2011, 21(7): 2183–2186
103. Presto S, Kumar P, Varma S, Viviani M, Singh P. Electrical conductivity of NiMo–based double perovskites under SOFC anodic conditions. International Journal of Hydrogen Energy, 2018, 43(9): 4528–4533
104. Fu D, Jin F, He T. A-site calcium-doped $Pr_{1-x}Ca_xBaCo_2O_{5+\delta}$ double perovskites as cathodes for intermediate-temperature solid oxide fuel cells. Journal of Power Sources, 2016, 313: 134–141
105. Anderson M T, Greenwood K B, Taylor G A, Poeppelmeier K. B-cation arrangements in double perovskites. Progress in Solid State Chemistry, 1993, 22(3): 197–233
106. Serrate D, De Teresa J M, Algarabel P A, Marquina C, Blasco J, Ibarra M R, Galibert J. Magnetoelastic coupling in $Sr_2(Fe_{1-x}Cr_x)$ ReO_6 double perovskites. Journal of Physics Condensed Matter, 2007, 19(43): 436226
107. Suntsov A Y, Leonidov I A, Patrakeev M V, Kozhevnikov V L. Defect formation in double perovskites $PrBaCo_{2-x}Cu_xO_{5+\delta}$ at elevated temperatures. Solid State Ionics, 2015, 274: 17–23
108. Niu B, Jin F, Yang X, Feng T, He T. Resisting coking and sulfur poisoning of double perovskite. 2018, 43(6): 3280–3290
109. Kim J H, Manthiram A. Layered $NdBaCo_{2-x}Ni_xO_{5+\delta}$ perovskite oxides as cathodes for intermediate temperature solid oxide fuel cells. Electrochimica Acta, 2009, 54(28): 7551–7557
110. Blasse G. New compounds with perovskite-like structures. Journal of Inorganic and Nuclear Chemistry, 1965, 27(5): 993–1003
111. Battle P D, Jones C W. The crystal and magnetic structures of Sr_2LuRuO_6, Ba_2YRuO_6, and Ba_2LuRuO_6. Journal of Solid State Chemistry, 1989, 78(1): 108–116
112. Azad A K, Ivanov S A, Eriksson S G, Eriksen J, Rundlöf H, Mathieu R, Svedlindh P. Synthesis, crystal structure, and magnetic characterization of the double perovskite Ba_2MnWO_6. Materials Research Bulletin, 2001, 36(12): 2215–2228
113. Azad A K, Eriksson S G, Mellergård A, Ivanov S A, Eriksen J, Rundlöf H. A study on the nuclear and magnetic structure of the double perovskites A_2FeWO_6 (A = Sr, Ba) by neutron powder diffraction and reverse Monte Carlo modeling. Materials Research Bulletin, 2002, 37(11): 1797–1813
114. Anderson M T, Poeppelmeier K R. La_2CuSnO_6: a new perovskite-

related compound with an unusual arrangement of B cations. Chemistry of Materials, 1991, 3(3): 476–482
115. Glazer A M. The classification of tilted octahedra in perovskites. Acta Crystallographica. Section B, Structural Crystallography and Crystal Chemistry, 1972, 28(11): 3384–3392
116. Blasse G. New compounds with perovskite-like structures. Journal of Inorganic and Nuclear Chemistry, 1965, 27(5): 993–1003
117. Prellier W, Smolyaninova V, Biswas A, Galley C, Greene R L, Ramesha K, Gopalakrishnan J. Properties of the ferrimagnetic double perovskites A_2FeReO_6 (A = Ba and Ca). Journal of Physics Condensed Matter, 2000, 12(6): 965–973
118. Anderson M T, Poeppelmeier K R. Lanthanum copper tin oxide (La_2CuSnO_6): a new perovskite-related compound with an unusual arrangement of B cations. Chemistry of Materials, 1991, 3(3): 476–482
119. Azad A K, Basheer F, Iskandar Petra P M, Ghosh A, Irvine J T S. Structure-property relationship in Mg-doped $La_{0.75}Sr_{0.25}Mn_{0.5}Cr_{0.5}O_3$ anode for solid oxide fuel cell. In: 5th Brunei International Conference on Engineering and Technology (BICET 2014), Bandar Seri Begawan, Brunei, 2014: 1115
120. Wang Y, Zhang H, Chen F, Xia C. Electrochemical characteristics of nano-structured $PrBaCo_2O_{5+x}$ cathodes fabricated with ion impregnation process. Journal of Power Sources, 2012, 203: 34–41
121. Ghosh A, Azad A K, Irvine J T S. Study of Ga doped LSCM as an anode for SOFC. ECS Transactions, 2011, 35(1): 1337–1343
122. Shaikh S P S, Muchtar A, Somalu M R. A review on the selection of anode materials for solid-oxide fuel cells. Renewable & Sustainable Energy Reviews, 2015, 51: 1–8
123. Xia C, Liu M. Microstructures, conductivities, and electrochemical properties of $Ce_{0.9}Gd_{0.1}O_2$ and GDC–Ni anodes for low-temperature SOFCs. Solid State Ionics, 2002, 152–153: 423–430
124. Brett D J L, Atkinson A, Brandon N P, Skinner S J. Intermediate temperature solid oxide fuel cells. Chemical Society Reviews, 2008, 37(8): 1568
125. Park S, Vohs J M, Gorte R J. Direct oxidation of hydrocarbons in a solid-oxide fuel cell. Nature, 2000, 404(6775): 265–267
126. Gorte R J, Vohs J M. Novel SOFC anodes for the direct electrochemical oxidation of hydrocarbons. Journal of Catalysis, 2003, 216(1–2): 477–486
127. Shri Prakash B, Senthil Kumar S, Aruna S T. Properties and development of Ni/YSZ as an anode material in solid oxide fuel cell: a review. Renewable & Sustainable Energy Reviews, 2014, 36: 149–179
128. Huan Y, Li Y, Yin B, Ding D, Wei T. High conductive and long-term phase stable anode materials for SOFCs: A_2FeMoO_6 (A = Ca, Sr, Ba). Journal of Power Sources, 2017, 359: 384–390
129. Zheng K, Świerczek K, Zając W, Klimkowicz A. Rock salt ordered-type double perovskite anode materials for solid oxide fuel cells. Solid State Ionics, 2014, 257: 9–16
130. Rath M K, Lee K T. Superior electrochemical performance of non-precious Co-Ni-Mo alloy catalyst-impregnated $Sr_2FeMoO_{6-\delta}$ as an electrode material for symmetric solid oxide fuel cells. Electrochimica Acta, 2016, 212: 678–685
131. dos Santos-Gómez L, León-Reina L, Porras-Vázquez J M, Losilla E R, Marrero-López D. Chemical stability and compatibility of double perovskite anode materials for SOFCs. Solid State Ionics, 2013, 239: 1–7
132. Kumar P, Presto S, Sinha A S K, Varma S, Viviani M, Singh P. Effect of samarium (Sm^{3+}) doping on structure and electrical conductivity of double perovskite Sr_2NiMoO_6 as anode material for SOFC. Journal of Alloys and Compounds, 2017, 725: 1123–1129
133. Ding H, Tao Z, Liu S, Yang Y. A redox-stable direct-methane solid oxide fuel cell (SOFC) with $Sr_2FeNb_{0.2}Mo_{0.8}O_{6-\delta}$ double perovskite as anode material. Journal of Power Sources, 2016, 327: 573–579
134. Sun Y F, Zhang Y Q, Hua B, Behnamian Y, Li J, Cui S H, Li J H, Luo J L. Molybdenum doped $Pr_{0.5}Ba_{0.5}MnO_{3-\delta}$ (Mo-PBMO) double perovskite as a potential solid oxide fuel cell anode material. Journal of Power Sources, 2016, 301: 237–241
135. Tomkiewicz A C, Tamimi M A, Huq A, McIntosh S. Structural analysis of $PrBaMn_2O_{5+\delta}$ under SOFC anode conditions by *in-situ* neutron powder diffraction. Journal of Power Sources, 2016, 330: 240–245
136. Xu L, Yin Y M, Zhou N, Wang Z, Ma Z F. Sulfur tolerant redox stable layered perovskite $SrLaFeO_{4-\delta}$ as anode for solid oxide fuel cells. Electrochemistry Communications, 2017, 76: 51–54
137. Wang F Y, Zhong G B, Luo S, Xia L, Fang L H, Song X, Hao X, Yan G. Porous $Sr_2MgMo_{1-x}V_xO_{6-d}$ ceramics as anode materials for SOFCs using biogas fuel. Catalysis Communications, 2015, 67: 108–111
138. He B, Wang Z, Zhao L, Pan X, Wu X, Xia C. Ti-doped molybdenum-based perovskites as anodes for solid oxide fuel cells. Journal of Power Sources, 2013, 241: 627–633
139. Escudero M J, Gómez deParada I, Fuerte A, Daza L. Study of $Sr_2Mg(Mo_{0.8}Nb_{0.2})O_{6-\delta}$ as anode material for solid oxide fuel cells using hydrocarbons as fuel. Journal of Power Sources, 2013, 243: 654–660
140. Zhang Q, Wei T, Huang Y H. Electrochemical performance of double-perovskite Ba_2MMoO_6 (M = Fe, Co, Mn, Ni) anode materials for solid oxide fuel cells. Journal of Power Sources, 2012, 198: 59–65
141. Marrero-López D, Peña-Martínez J, Ruiz-Morales J C, Martín-Sedeño M C, Núñez P. High temperature phase transition in SOFC anodes based on $Sr_2MgMoO_{6-\delta}$. Journal of Solid State Chemistry, 2009, 182(5): 1027–1034
142. Han Z, Wang Y, Yang Y, Li L, Yang Z, Han M. High-performance SOFCs with impregnated $Sr_2Fe_{1.5}Mo_{0.5}O_{6-\delta}$ anodes toward sulfur resistance. Journal of Alloys and Compounds, 2017, 703: 258–263
143. Gansor P, Xu C, Sabolsky K, Zondlo J W, Sabolsky E M. Phosphine impurity tolerance of $Sr_2MgMoO_{6-\delta}$ composite SOFC anodes. Journal of Power Sources, 2012, 198: 7–13
144. Li H, Zhao Y, Wang Y, Li Y. $Sr_2Fe_{2-x}Mo_xO_{6-\delta}$ perovskite as an anode in a solid oxide fuel cell: effect of the substitution ratio. Catalysis Today, 2016, 259: 417–422
145. Zhang L, Zhou Q, He Q, He T. Double-perovskites $A_2FeMoO_{6-\delta}$ (A = Ca, Sr, Ba) as anodes for solid oxide fuel cells. Journal of Power Sources, 2010, 195(19): 6356–6366
146. Jiang L, Liang G, Han J, Huang Y. Effects of Sr-site deficiency on structure and electrochemical performance in Sr_2MgMoO_6 for solid-oxide fuel cell. Journal of Power Sources, 2014, 270: 441–448

147. Marrero-López D, Peña-Martínez J, Ruiz-Morales J C, Gabás M, Núñez P, Aranda M A G, Ramos-Barrado J R. Redox behaviour, chemical compatibility and electrochemical performance of $Sr_2MgMoO_{6-\delta}$ as SOFC anode. Solid State Ionics, 2010, 180 (40): 1672–1682
148. Howell T G, Kuhnell C P, Reitz T L, Sukeshini A M, Singh R N. $\{A_2MgMoO_6\}$ (A = Sr,Ba) for use as sulfur tolerant anodes. Journal of Power Sources, 2013, 231: 279–284
149. Zhang P, Huang Y H, Cheng J G, Mao Z Q, Goodenough J B. Sr_2CoMoO_6 anode for solid oxide fuel cell running on H_2 and CH_4 fuels. Journal of Power Sources, 2011, 196(4): 1738–1743
150. Vasala S, Lehtimäki M, Haw S C, Chen J M, Liu R S, Yamauchi H, Karppinen M. Isovalent and aliovalent substitution effects on redox chemistry of $Sr_2MgMoO_{6-\delta}$ SOFC-anode material. Solid State Ionics, 2010, 181(15–16): 754–759
151. Liu Q, Bugaris D E, Xiao G, Chmara M, Ma S, zur Loye H C, Amiridis M D, Chen F. $Sr_2Fe_{1.5}Mo_{0.5}O_{6-\delta}$ as a regenerative anode for solid oxide fuel cells. Journal of Power Sources, 2011, 196(22): 9148–9153
152. Karim A H, Park K Y, Lee T H, Muhammed Ali S A, Hossain S, Absah H Q H H, Park J Y, Azad A K. Synthesis, structure and electrochemical performance of double perovskite oxide $Sr_2Fe_{1-x}Ti_xNbO_{6-\delta}$ as SOFC electrode. Journal of Alloys and Compounds, 2017, 724: 666–673
153. Martínez-Coronado R, Aguadero A, Alonso J A, Fernández-Díaz M T. Reversible oxygen removal and uptake in the La_2ZnMnO_6 double perovskite: performance in symmetrical SOFC cells. Solid State Sciences, 2013, 18: 64–70
154. Li W, Cheng Y, Zhou Q, Wei T, Li Z, Yan H, Wang Z, Han X. Evaluation of double perovskite $Sr_2FeTiO_{6-\delta}$ as potential cathode or anode materials for intermediate-temperature solid oxide fuel cells. Ceramics International, 2015, 41(9): 12393–12400
155. Ding H, Sullivan N P, Ricote S. Double perovskite $Ba_2FeMoO_{6-\delta}$ as fuel electrode for protonic-ceramic membranes. Solid State Ionics, 2017, 306: 97–103
156. Zheng K, Świerczek K, Bratek J, Klimkowicz A. Cation-ordered perovskite-type anode and cathode materials for solid oxide fuel cells. Solid State Ionics, 2014, 262: 354–358
157. Song Y, Zhong Q, Tan W, Pan C. Effect of cobalt-substitution $Sr_2Fe_{1.5-x}Co_xMo_{0.5}O_{6-\delta}$ for intermediate temperature symmetrical solid oxide fuel cells fed with H_2-H_2S. Electrochimica Acta, 2014, 139: 13–20
158. Tarancón A, Marrero-López D, Peña-Martínez J, Ruizmorales J, Nunez P. Effect of phase transition on high-temperature electrical properties of $GdBaCo_2O_{5+x}$ layered perovskite. Solid State Ionics, 2008, 179(17–18): 611–618
159. Song Y, Zhong Q, Wang D, Xu Y, Tan W. Interaction between electrode materials $Sr_2FeCo_{0.5}Mo_{0.5}O_{6-\delta}$ and hydrogen sulfide in symmetrical solid oxide fuel cells. International Journal of Hydrogen Energy, 2017, 42(34): 22266–22272
160. Wright J H, Virkar A V, Liu Q, Chen F. Electrical characterization and water sensitivity of $Sr_2Fe_{1.5}Mo_{0.5}O_{6-\delta}$ as a possible solid oxide fuel cell electrode. Journal of Power Sources, 2013, 237: 13–18
161. Kim J H, Cassidy M, Irvine J T S, Bae J. Advanced electrochemical properties of $LnBa_{0.5}Sr_{0.5}Co_2O_{5+\delta}$ (Ln = Pr, Sm, and Gd) as cathode materials for IT-SOFC. Journal of the Electrochemical Society, 2009, 156(6): B682–B689
162. Haile S M. Fuel cell materials and components. Acta Materialia, 2003, 51(19): 5981–6000
163. Jiang S P. Issues on development of $(La,Sr)MnO_3$ cathode for solid oxide fuel cells. Journal of Power Sources, 2003, 124(2): 390–402
164. Carter S, Selcuk A, Chater R J, Kajda J, Kilner J A, Steele B C H. Oxygen transport in selected nonstoichiometric perovskite-structure oxides. Solid State Ionics, 1992, 53–56: 597–605
165. Kim G, Wang S, Jacobson A J, Reimus L, Brodersen P, Mims C A. Rapid oxygen ion diffusion and surface exchange kinetics in $PrBaCo_2O_{5+x}$ with a perovskite related structure and ordered A cations. Journal of Materials Chemistry, 2007, 17(24): 2500
166. Choi S, Kucharczyk C J, Liang Y, Zhang X, Takeuchi I, Ji H I, Haile S M. Exceptional power density and stability at intermediate temperatures in protonic ceramic fuel cells. Nature Energy, 2018, 3 (3): 202–210
167. Sun C, Hui R, Roller J. Cathode materials for solid oxide fuel cells: a review. Journal of Solid State Electrochemistry, 2010, 14(7): 1125–1144
168. Lü S, Meng X, Ji Y, Fu C, Sun C, Zhao H. Electrochemical performances of $NdBa_{0.5}Sr_{0.5}Co_2O_{5+x}$ as potential cathode material for intermediate-temperature solid oxide fuel cells. Journal of Power Sources, 2010, 195(24): 8094–8096
169. Jiang X, Wang J, Jia G, Qie Z, Shi Y, Idrees A, Zhang Q, Jiang L. Characterization of $PrBa_{0.92}CoCuO_{6-\delta}$ as a potential cathode material of intermediate-temperature solid oxide fuel cell. International Journal of Hydrogen Energy, 2017, 42(9): 6281–6289
170. Tomkiewicz A C, Meloni M, McIntosh S. On the link between bulk structure and surface activity of double perovskite based SOFC cathodes. Solid State Ionics, 2014, 260: 55–59
171. Li H, Sun L P, Li Q, Xia T, Zhao H, Huo L H, Bassat J M, Rougier A, Fourcade S, Grenier J C. Electrochemical performance of double perovskite Pr_2NiMnO_6 as a potential IT-SOFC cathode. International Journal of Hydrogen Energy, 2015, 40(37): 12761–12769
172. Mao X, Wang W, Ma G. A novel cobalt-free double-perovskite $NdBaFe_{1.9}Nb_{0.1}O_{5+\delta}$ cathode material for proton-conducting IT-SOFC. Ceramics International, 2015, 41(8): 10276–10280
173. Jin F J, Liu J, Niu B, Ta L, Li R, Wang Y, Yang X, He T. Evaluation and performance optimization of double-perovskite $LaSrCoTiO_{5+\delta}$ cathode for intermediate-temperature solid-oxide fuel cells. International Journal of Hydrogen Energy, 2016, 41(46): 21439–21449
174. Fu D, Jin F, He T. A-site calcium-doped $Pr_{1-x}Ca_xBaCo_2O_{5+\delta}$ double perovskites as cathodes for intermediate-temperature solid oxide fuel cells. Journal of Power Sources, 2016, 313: 134–141
175. Pelosato R, Cordaro G, Stucchi D, Cristiani C, Dotelli G. Cobalt based layered perovskites as cathode material for intermediate temperature solid oxide fuel cells : a brief review. Journal of Power Sources, 2015, 298: 46–67
176. Mao X, Yu T, Ma G. Performance of cobalt-free double-perovskite $NdBaFe_{2-x}Mn_xO_{5+\delta}$ cathode materials for proton-conducting IT-SOFC. Journal of Alloys and Compounds, 2015, 637: 286–290
177. Pang S, Wang W, Chen T, Wang Y, Xu K, Shen X, Xi X, Fan J. The effect of potassium on the properties of $PrBa_{1-x}Co_2O_{5+\delta}$ (x = 0.00–0.10) cathodes for intermediate-temperature solid oxide fuel

cells. International Journal of Hydrogen Energy, 2016, 41(31): 13705–13714

178. Xia L N, He Z P, Huang X W, Yu Y. Synthesis and properties of $SmBaCo_{2-x}Ni_xO_{5+\delta}$ perovskite oxide for IT-SOFC cathodes. Ceramics International, 2016, 42(1): 1272–1280
179. Jin F, Xu H, Long W, Shen Y, He T. Characterization and evaluation of double perovskites $LnBaCoFeO_{5+\delta}$ (Ln = Pr and Nd) as intermediate-temperature solid oxide fuel cell cathodes. Journal of Power Sources, 2013, 243: 10–18
180. Seymour I D, Tarancón A, Chroneos A, Parfitt D, Kilner J A, Grimes R W. Anisotropic oxygen diffusion in $PrBaCo_2O_{5.5}$ double perovskites. Solid State Ionics, 2012, 216: 41–43
181. Suntsov A Y, Leonidov I A, Patrakeev M V, Kozhevnikov V L. Defect formation in double perovskites $PrBaCo_{2-x}Cu_xO_{5+\delta}$ at elevated temperatures. Solid State Ionics, 2015, 274: 17–23
182. Saccoccio M, Jiang C, Gao Y, Chen D, Ciucci F. Nb-substituted $PrBaCo_2O_{5+\delta}$ as a cathode for solid oxide fuel cells: a systematic study of structural, electrical, and electrochemical properties. International Journal of Hydrogen Energy, 2017, 42(30): 19204–19215
183. Jin F, Li L, He T. $NdBaCo_{2/3}Fe_{2/3}Cu_{2/3}O_{5+\delta}$ double perovskite as a novel cathode material for CeO_2- and $LaGaO_3$-based solid oxide fuel cells. Journal of Power Sources, 2015, 273: 591–599
184. Li L, Jin F, Shen Y, He T. Cobalt-free double perovskite cathode $GdBaFeNiO_{5+\delta}$ and electrochemical performance improvement by $Ce_{0.8}Sm_{0.2}O_{1.9}$ impregnation for intermediate-temperature solid oxide fuel cells. Electrochimica Acta, 2015, 182: 682–692
185. Li S, Xia T, Li Q, Sun L, Huo L, Zhao H. *A*-site Ba-deficiency layered perovskite $EuBa_{1-x}Co_2O_{6-\delta}$ cathodes for intermediate-temperature solid oxide fuel cells: electrochemical properties and oxygen reduction reaction kinetics. International Journal of Hydrogen Energy, 2017, 42(38): 24412–24425
186. Jin F, Shen Y, Wang R, He T. Double-perovskite $PrBaCo_{2/3}Fe_{2/3}Cu_{2/3}O_{5+\delta}$ as cathode material for intermediate-temperature solid-oxide fuel cells. Journal of Power Sources, 2013, 234: 244–251
187. Meng F, Xia T, Wang J, Shi Z, Zhao H. Praseodymium-deficiency $Pr_{0.94}BaCo_2O_{6-\delta}$ double perovskite: a promising high performance cathode material for intermediate-temperature solid oxide fuel cells. Journal of Power Sources, 2015, 293: 741–750
188. Jin F, Liu J, Shen Y, He T. Improved electrochemical performance and thermal expansion compatibility of $LnBaCoFeO_{5+\delta}Sm_{0.2}Ce_{0.8}O_{1.9}$ (Ln = Pr and Nd) composite cathodes for IT-SOFCs. Journal of Alloys and Compounds, 2016, 685: 483–491
189. Xue J, Shen Y, He T. Double-perovskites $YBaCo_{2-x}Fe_xO_{5+\delta}$ cathodes for intermediate-temperature solid oxide fuel cells. Journal of Power Sources, 2011, 196(8): 3729–3735
190. Zhou Q, He T, Ji Y. $SmBaCo_2O_{5+x}$ double-perovskite structure cathode material for intermediate-temperature solid-oxide fuel cells. Journal of Power Sources, 2008, 185(2): 754–758
191. Kong X, Liu G, Yi Z, Ding X. $NdBaCu_2O_{5+\delta}$ and $NdBa_{0.5}Sr_{0.5}Cu_2O_{5+\delta}$ layered perovskite oxides as cathode materials for IT-SOFCs. International Journal of Hydrogen Energy, 2015, 40(46): 16477–16483
192. Wei B, Chen K, Wang C C, Lü Z, Jiang S P. Performance degradation of $SmBaCo_2O_{5+\delta}$ cathode induced by chromium deposition for solid oxide fuel cells. Electrochimica Acta, 2015, 174: 327–331
193. Lü S, Yu B, Meng X, Zhang Y, Ji Y, Fu C, Yang L, Li X, Sui Y, Yang J. Performance of double-perovskite $YBa_{0.5}Sr_{0.5}Co_{1.4}Cu_{0.6}O_{5+\delta}$ as cathode material for intermediate-temperature solid oxide fuel cells. Ceramics International, 2014, 40(9, Part B): 14919–14925
194. Kuroda C, Zheng K, Swierczek K. Characterization of novel $GdBa_{0.5}Sr_{0.5}Co_{2-x}Fe_xO_{5+\delta}$ perovskites for application in IT-SOFC cells. International Journal of Hydrogen Energy, 2013, 38(2): 1027–1038
195. Subardi A, Chen C C, Cheng M H, Chang W K, Fu Y P. Electrical, thermal and electrochemical properties of $SmBa_{1-x}Sr_xCo_2O_{5+\delta}$ cathode materials for intermediate-temperature solid oxide fuel cells. Electrochimica Acta, 2016, 204: 118–127
196. Yu L, Chen Y, Gu Q, Tian D, Lu X, Meng G, Lin B. Layered perovskite oxide $Y_{0.8}Ca_{0.2}BaCoFeO_{5+\delta}$ as a novel cathode material for intermediate-temperature solid oxide fuel cells. Journal of Rare Earths, 2015, 33(5): 519–523 (in Chinese)
197. Donazzi A, Pelosato R, Cordaro G, Stucchi D, Cristiani C, Dotelli G, Sora I N. Evaluation of Ba deficient $NdBaCo_2O_{5+\delta}$ oxide as cathode material for IT-SOFC. Electrochimica Acta, 2015, 182: 573–587
198. Che X, Shen Y, Li H, He T. Assessment of $LnBaCo_{1.6}Ni_{0.4}O_{5+\delta}$ (Ln = Pr, Nd, and Sm) double-perovskites as cathodes for intermediate-temperature solid-oxide fuel cells. Journal of Power Sources, 2013, 222: 288–293
199. Pérez-Flores J C, Gómez-Pérez A, Yuste M, Canales-Vázquez J, Climent-Pascual E, Ritter C, Azcondo M T, Amador U, García-Alvarado F. Characterization of $La_{2-x}Sr_xCoTiO_6$ ($0.6 \leqslant x \leqslant 1.0$) series as new cathodes of solid oxide fuel cells. International Journal of Hydrogen Energy, 2014, 39(10): 5440–5450
200. Wang W, Pang S, Su Y, Shen X, Wang Y, Xu K, Xi X, Xiang J. The effect of calcium on the properties of $SmBa_{1-x}Ca_xCoCuO_{5+\delta}$ as a cathode material for intermediate-temperature solid oxide fuel cells. Journal of the European Ceramic Society, 2017, 37(4): 1557–1562
201. Cascos V, Troncoso L, Alonso J A. New families of M^{n+}-doped $SrCo_{1-x}M_xO_{3-\delta}$ perovskites performing as cathodes in solid-oxide fuel cells. International Journal of Hydrogen Energy, 2015, 40(34): 11333–11341
202. Zhu Z, Tao Z, Bi L, Liu W. Investigation of $SmBaCuCoO_{5+\delta}$ double-perovskite as cathode for proton-conducting solid oxide fuel cells. Materials Research Bulletin, 2010, 45(11): 1771–1774
203. Pang S L, Jiang X N, Li X N, Xu H X, Jiang L, Xu Q L, Shi Y C, Zhang Q Y. Structure and properties of layered-perovskite $LaBa_{1-x}Co_2O_{5+\delta}$ (x = 0–0.15) as intermediate-temperature cathode material. Journal of Power Sources, 2013, 240: 54–59
204. Dai N, Wang Z, Jiang T, Feng J, Sun W, Qiao J, Rooney D, Sun K. A new family of barium-doped $Sr_2Fe_{1.5}Mo_{0.5}O_{6-\delta}$ perovskites for application in intermediate temperature solid oxide fuel cells. Journal of Power Sources, 2014, 268: 176–182
205. Tsvetkova N S, Zuev A Y, Tsvetkov D S. Investigation of $GdBaCo_{2-x}Fe_xO_{6-\delta}$ (x = 0, 0.2)-$Ce_{0.8}Sm_{0.2}O_2$ composite cathodes for intermediate temperature solid oxide fuel cells. Journal of Power Sources, 2013, 243: 403–408

206. Zhou Q, Wei W C J, Guo Y, Jia D. $LaSrMnCoO_{5+\delta}$ as cathode for intermediate-temperature solid oxide fuel cells. Electrochemistry Communications, 2012, 19: 36–38
207. Jiang X, Xu Q, Shi Y, Li X, Zhou W, Xu H, Zhang Q. Synthesis and properties of Sm^{3+}-deficient $Sm_{1-x}BaCo_2O_{5+\delta}$ perovskite oxides as cathode materials. International Journal of Hydrogen Energy, 2014, 39(21): 10817–10823
208. Zhen S, Sun W, Tang G, Rooney D, Sun K, Ma X. Evaluation of strontium-site-deficient $Sr_2Fe_{1.4}Co_{0.1}Mo_{0.5}O_{6-\delta}$-based perovskite oxides as intermediate temperature solid oxide fuel cell cathodes. International Journal of Hydrogen Energy, 2016, 41(22): 9538–9546
209. Zhang K, Ge L, Ran R, Shao Z, Liu S. Synthesis, characterization and evaluation of cation-ordered $LnBaCo_2O_{5+\delta}$ as materials of oxygen permeation membranes and cathodes of SOFCs. Acta Materialia, 2008, 56(17): 4876–4889
210. Gómez-Pérez A, Yuste M, Pérez-Flores J C, Ritter C, Azcondo M T, Canales-Vázquez J, Gálvez-Sánchez M, Boulahya K, García-Alvarado F, Amador U. The role of the Co^{2+}/Co^{3+} redox-pair in the properties of $La_{2-x}Sr_xCoTiO_6$ ($0 \leqslant x \leqslant 0.5$) perovskites as components for solid oxide fuel cells. Journal of Power Sources, 2013, 227: 309–317
211. Wang B, Long G, Ji Y, Pang M, Meng X. Layered perovskite $PrBa_{0.5}S_{r0.5}CoCuO_{5+\delta}$ as a cathode for intermediate-temperature solid oxide fuel cells. Journal of Alloys and Compounds, 2014, 606: 92–96
212. Yi K, Sun L, Li Q, Xia T, Huo L, Zhao H, Li J, Lü Z, Bassat J M, Rougier A, Fourcade S, Grenier J C. Effect of Nd-deficiency on electrochemical properties of $NdBaCo_2O_{6-\delta}$ cathode for intermediate-temperature solid oxide fuel cells. International Journal of Hydrogen Energy, 2016, 41(24): 10228
213. Zhou Q, Cheng Y, Li W, Yang X, Liu J, An D, Tong X, Zhong B, Wang W. Investigation of cobalt-free perovskite $Sr_2FeTi_{0.75}Mo_{0.25}O_{6-\delta}$ as new cathode for solid oxide fuel cells. Materials Research Bulletin, 2016, 74: 129–133
214. Xue J, Shen Y, He T. Performance of double-proveskite $YBa_{0.5}Sr_{0.5}Co_2O_{5+\delta}$ as cathode material for intermediate-temperature solid oxide fuel cells. International Journal of Hydrogen Energy, 2011, 36(11): 6894–6898
215. Wang Y, Zhao X, Lü S, Meng X, Zhang Y, Yu B, Li X, Sui Y, Yang J, Fu C, Ji Y. Synthesis and characterization of $SmSrCo_{2-x}Mn_xO_{5+\delta}$ ($x = 0.0$, 0.2, 0.4, 0.6, 0.8, 1.0) cathode materials for intermediate-temperature solid-oxide fuel cells. Ceramics International, 2014, 40(7): 11343–11350
216. Lü S, Long G, Meng X, Ji Y, Lü B, Zhao H. $PrBa_{0.5}Sr_{0.5}Co_2O_{5+x}$ as cathode material based on LSGM and GDC electrolyte for intermediate-temperature solid oxide fuel cells. International Journal of Hydrogen Energy, 2012, 37(7): 5914–5919
217. Lee S J, Kim D S, Jo S H, Muralidharan P, Kim D K. Electrochemical properties of $GdBaCo_{2/3}Fe_{2/3}Cu_{2/3}O_{5+}$-CGO composite cathodes for solid oxide fuel cell. Ceramics International, 2012, 38(Sup.1): S493–496
218. Li X, Jiang X, Xu H, Xu Q, Jiang L, Shi Y, Zhang Q. Scandium-doped $PrBaCo_{2-x}Sc_xO_{6-\delta}$ oxides as cathode material for intermediate-temperature solid oxide fuel cells. International Journal of Hydrogen Energy, 2013, 38(27): 12035–12042
219. Choi S, Shin J, Kim G. The electrochemical and thermodynamic characterization of $PrBaCo_{2-x}Fe_xO_{5+\delta}$ ($x = 0$, 0.5, 1) infiltrated into yttria-stabilized zirconia scaffold as cathodes for solid oxide fuel cells. Journal of Power Sources, 2012, 201: 10–17
220. Zhu C, Liu X, Yi C, Yan D, Su W. Electrochemical performance of $PrBaCo_2O_{5+\delta}$ layered perovskite as an intermediate-temperature solid oxide fuel cell cathode. Journal of Power Sources, 2008, 185 (1): 193–196
221. Tarancón A, Morata A, Dezanneau G, Skinner S J, Kilner J A, Estradé S, Hernández-Ramírez F, Peiró F, Morante J R. $GdBaCo_2O_{5+x}$ layered perovskite as an intermediate temperature solid oxide fuel cell cathode. Journal of Power Sources, 2007, 174 (1): 255–263
222. Ding H, Xue X, Liu X, Meng G. High performance layered $SmBa_{0.5}Sr_{0.5}Co_2O_{5+\delta}$ cathode for intermediate-temperature solid oxide fuel cells. Journal of Power Sources, 2009, 194(2): 815–817
223. Hou M, Sun W, Li P, Feng J, Yang G, Qiao J, Wang Z, Rooney D, Feng J, Sun K. Investigation into the effect of molybdenum-site substitution on the performance of $Sr_2Fe_{1.5}Mo_{0.5}O_{6-\delta}$ for intermediate temperature solid oxide fuel cells. Journal of Power Sources, 2014, 272: 759–765
224. Li X, Jiang X, Shi Y, Zhou W, Xu Q, Xu H, Zhang Q. One-step synthesized nano-composite cathode material of $Pr_{0.83}BaCo_{1.33}Sc_{0.5}O_{6-\delta}$–0.17$PrCoO_3$ for intermediate-temperature solid oxide fuel cell. International Journal of Hydrogen Energy, 2014, 39(27): 15039–15045
225. Zou J, Park J, Kwak B, Yoon H, Chung J. Effect of Fe doping on $PrBaCo_2O_{5+\delta}$ as cathode for intermediate-temperature solid oxide fuel cells. Solid State Ionics, 2012, 206: 112–119
226. Zhang Y, Yu B, Lu S, Meng X, Zhao X, Ji Y, Wang Y, Fu C, Liu X, Li X, Sui Y, Lang J, Yang J. Effect of Cu doping on $YBaCo_2O_{5+\delta}$ as cathode for intermediate-temperature solid oxide fuel cells. Electrochimica Acta, 2014, 134: 107–115
227. Lü S, Long G, Ji Y, Meng X, Zhao H, Sun C. $SmBaCoCuO_{5+x}$ as cathode material based on GDC electrolyte for intermediate-temperature solid oxide fuel cells. Journal of Alloys and Compounds, 2011, 509(6): 2824–2828
228. Azad A K, Kim J H, Irvine J T S. Structure–property relationship in layered perovskite cathode $LnBa_{0.5}Sr_{0.5}Co_2O_{5+\delta}$ (Ln = Pr, Nd) for solid oxide fuel cells. Journal of Power Sources, 2011, 196(17): 7333–7337
229. Hu Y, Bogicevic C, Bouffanais Y, Giot M, Hernandez O, Dezanneau G. Synthesis, physical-chemical characterization and electrochemical performance of $GdBaCo_{2-x}Ni_xO_{5+\delta}$ (x = 0–0.8) as cathode materials for IT-SOFC application. Journal of Power Sources, 2013, 242: 50–56
230. Xia T, Lin N, Zhao H, Huo L, Wang J, Grenier J C. Co-doped Sr_2FeNbO_6 as cathode materials for intermediate-temperature s olid oxide fuel cells. Journal of Power Sources, 2009, 192(2): 291–296
231. Subardi A, Cheng M H, Fu Y P. Chemical bulk diffusion and electrochemical properties of $SmBa_{0.6}Sr_{0.4}Co_2O_{5+\delta}$ cathode for intermediate solid oxide fuel cells. International Journal of Hydrogen Energy, 2014, 39(35): 20783–20790

232. Mitchell R H. Perovskites : Modern and Ancient. Ontario, Canada: Almaz Press, 2002
233. Horita T, Kishimoto H, Yamaji K, Brito M E, Xiong Y, Yokokawa H, Hori Y, Miyachi I. Effects of impurities on the degradation and long-term stability for solid oxide fuel cells. Journal of Power Sources, 2009, 193(1): 194–198
234. Tao S W, Irvine J T S. A redox-stable efficient anode for solid-oxide fuel cells. Nature Materials, 2003, 2(5): 320–323
235. Fu Q X, Tietz F. Ceramic-based anode materials for improved redox cycling of solid oxide fuel cells. Fuel Cells (Weinheim), 2008, 8(5): 283–293
236. Azad A K, Hakem A, Iskandar Petra P M. Titanium doped LSCM anode for hydrocarbon fuelled SOFCs. AIP Conference Proceedings, 2015, 070069
237. Tao S W, Canales-Vazquez J, Irvine J T S. Structural and electrical properties of the perovskite oxide Sr_2FeNbO_6. Chemistry of Materials, 2004, 16(11): 2309–2316
238. Téllez Lozano H, Druce J, Cooper S J, Kilner J A. Double perovskite cathodes for proton-conducting ceramic fuel cells: are they triple mixed ionic electronic conductors? Science and Technology of Advanced Materials, 2017, 18(1): 977–986
239. Peña-Martínez J, Marrero-López D, Ruiz-Morales J C, Savaniu C, Núñez P, Irvine J T S. Anodic performance and intermediate temperature fuel cell testing of $La_{0.75}Sr_{0.25}Cr_{0.5}Mn_{0.5}O_{3-\delta}$ at lanthanum gallate electrolytes. Chemistry of Materials, 2006, 18 (4): 1001–1006
240. Danilovic N, Luo J L, Chuang K T, Sanger A R. $Ce_{0.9}Sr_{0.1}VO_x$ (x = 3, 4) as anode materials for H_2S-containing {CH_4} fueled solid oxide fuel cells. Journal of Power Sources, 2009, 192(2): 247–257
241. Azad A K, Irvine J T S. Characterization of $YSr_2Fe_3O_{8-\delta}$ as electrode materials for SOFC. Solid State Ionics, 2011, 192(1): 225–228
242. Huang Y H, Liang G, Croft M, Lehtimäki M, Karppinen M, Goodenough J B. Double-perovskite anode materials Sr_2MMoO_6 (M = Co, Ni) for solid oxide fuel cells. Chemistry of Materials, 2009, 21(11): 2319–2326
243. Ralph J M, Schoeler A C, Krumpelt M. Materials for lower temperature solid oxide fuel cells. Electrochemical Technology, 2001, 6(5): 1161–1172
244. Adler S B. Factors governing oxygen reduction in solid oxide fuel cell cathodes. Chemical Reviews, 2004, 104(10): 4791–4844
245. Tao S W, Irvine J T S. Synthesis and characterization of $(La_{0.75}Sr_{0.25})Cr_{0.5}Mn_{0.5}O_{3-\delta}$, a redox-stable, efficient perovskite anode for SOFCs. Journal of the Electrochemical Society, 2004, 151(2): A252
246. Tao S W, Irvine J T S. Catalytic properties of the perovskite oxide $La_{0.75}Sr_{0.25}Cr_{0.5}Fe_{0.5}O_{3-\delta}$ in relation to its potential as a solid oxide fuel cell anode material. Chemistry of Materials, 2004, 16 (21): 4116–4121
247. Ruiz-Morales J C, Canales-Vázquez J, Savaniu C, Marrero-López D, Zhou W, Irvine J T S. Disruption of extended defects in solid oxide fuel cell anodes for methane oxidation. Nature, 2006, 439 (7076): 568–571
248. Zhu W Z, Deevi S C. A review on the status of anode materials for solid oxide fuel cells. Materials Science and Engineering A, 2003, 362(1–2): 228–239
249. Fagg D P, Kharton V V, Kovalevsky A V, Viskup A P, Naumovich E N, Frade J R. The stability and mixed conductivity in La and Fe doped $SrTiO_3$ in the search for potential {SOFC} anode materials. Journal of the European Ceramic Society, 2001, 21(10–11): 1831–1835
250. Touleva A, Yufit V, Simons S, Maskell W C, Brett D J L. A review of liquid metal anode solid oxide fuel cells. Journal of Electrochemical Science and Engineering, 2013, 3(3): 91–105
251. Wang X, Yu B, Zhang W, Chen J, Luo X, Stephan K. Microstructural modification of the anode/electrolyte interface of SOEC for hydrogen production. International Journal of Hydrogen Energy, 2012, 37(17): 12833–12838
252. dos Santos-Gómez L, León-Reina L, Porras-Vázquez J M, Losilla E R, Marrero-López D. Chemical stability and compatibility of double perovskite anode materials for SOFCs. Solid State Ionics, 2013, 239: 1–7
253. Saines P J, Kennedy B J. Phase segregation in mixed Nb–Sb double perovskites $Ba_2LnNb_{1-x}Sb_xO_{6-\delta}$. Journal of Solid State Chemistry, 2008, 181(2): 298–305
254. Tonus F, Bahout M, Dorcet V, Sharma R K, Djurado E, Paofai S, Smith R I, Skinner S J. A-site order–disorder in the $NdBaMn_2O_{5+\delta}$ SOFC electrode material monitored in situ by neutron diffraction under hydrogen flow. Journal of Materials Chemistry. A, Materials for Energy and Sustainability, 2017, 5(22): 11078–11085
255. Deng Z Q, Smit J P, Niu H J, Evans G, Li M R, Xu Z L, Claridge J B, Rosseinsky M J. B cation ordered double perovskite $Ba_2CoMo_{0.5}Nb_{0.5}O_{6-\delta}$ as a potential SOFC cathode. Chemistry of Materials, 2009, 21(21): 5154–5162
256. Afroze S, Abdalla A M, Radenahmad N, et al. Synthesis, structural and thermal properties of double perovskite $NdSrMn_2O_6$ as potential anode materials for solid oxide fuel cells. In: 7th Brunei International Conference on Engineering and Technology 2017 (BICET 2017), Antalya, Turkey, 2018
257. Falcón H, Barbero J A, Araujo G, Casais M T, Martínez-Lope M J, Alonso J A, Fierro J L G. Double perovskite oxides $A_2FeMoO_{6-\delta}$ (A = Ca, Sr and Ba) as catalysts for methane combustion. Applied Catalysis B: Environmental, 2004, 53(1): 37–45
258. Philipp B, Majewski P, Alff L, Erb A, Gross R, Graf T, Brandt M S, Simon J, Walther T, Mader W, Topwal D, Sarma D D. Structural and doping effects in the half-metallic double perovskite A_2CrWO_6 (A = Sr, Ba, and Ca). Physical Review B: Condensed Matter and Materials Physics, 2003, 68(14): 144431
259. Karim A H, Park K Y, Lee T H, Muhammed Ali S A, Hossain S, Absah H Q H H, Park J Y, Azad A K. Synthesis, structure and electrochemical performance of double perovskite oxide $Sr_2Fe_{1-x}Ti_xNbO_{6-\delta}$ as SOFC electrode. Journal of Alloys and Compounds, 2017, 724: 666–673
260. Zhang L, He T. Performance of double-perovskite $Sr_{2-x}Sm_xMgMoO_{6-\delta}$ as solid-oxide fuel-cell anodes. Journal of Power Sources, 2011, 196(20): 8352–8359
261. Zhang L L, Zhou Q J, He Q, He T. Double-perovskites $A_2FeMoO_{6-\delta}$ (A = Ca, Sr, Ba) as anodes for solid oxide fuel cells. Journal of Power Sources, 2010, 195(19): 6356–6366
262. Pickett W E. Spin-density-functional-based search for half-metallic antiferromagnets. Physical Review. B, 1998, 57(17): 10613–10619